

# Continual learning under domain transfer with sparse synaptic bursting

Shawn L. Beaulieu<sup>a,d,e</sup>, Jeff Clune<sup>c,f</sup>, and Nick Cheney<sup>b,d,e</sup>

<sup>a</sup>shawn.beaulieu@uvm.edu; <sup>b</sup>ncheney@uvm.edu; <sup>c</sup>jclune@gmail.com; <sup>d</sup>Department of Computer Science, University of Vermont: Burlington, VT, USA; <sup>e</sup>Vermont Complex Systems Center; <sup>f</sup>Department of Computer Science, University of British Columbia: Vancouver, BC, Canada

**Existing machines are functionally specific tools that were made for easy prediction and control. Tomorrow’s machines may be closer to biological systems in their mutability, resilience, and autonomy. But first they must be capable of learning, and retaining, new information without repeated exposure to it. Past efforts to engineer such systems have sought to build or regulate artificial neural networks using task-specific modules with constrained circumstances of application. This has not yet enabled continual learning over long sequences of previously unseen data without corrupting existing knowledge—a problem known as catastrophic forgetting. In this paper, we introduce a system that can learn sequentially over previously unseen datasets (ImageNet, CIFAR-100) with little forgetting over time. This is accomplished by regulating the activity of weights in a convolutional neural network on the basis of inputs using top-down modulation generated by a second feed-forward neural network. We find that our method learns continually under domain transfer with sparse bursts of activity in weights that are recycled across tasks, rather than by maintaining task-specific modules. Sparse synaptic bursting is found to balance enhanced and diminished activity in a way that facilitates adaptation to new inputs without corrupting previously acquired functions. This behavior emerges during a prior meta-learning phase in which regulated synapses are selectively disinhibited, or grown, from an initial state of uniform suppression.**

machine learning | catastrophic forgetting | cybernetics

Catastrophic forgetting is the phenomenon wherein an artificial neural network trained over a sequence of tasks loses its ability to perform a function it acquired earlier in the sequence as new information is learned (1, 2). This happens because the network’s ability to perform a given function is determined by the values of its synapses. Changes to these values, as a consequence of learning, may corrupt functions that are not robust to perturbation. But resistance to change when existing knowledge is insufficient to solve future problems will lead to failure.

In cases where data storage is secured through some external process, forgetting can be solved by removing the sequential character of learning with large batches of randomly ordered input (3). Meanwhile, defective knowledge can always be rectified by ever more optimization, because previously learned inputs can be revisited arbitrarily often. But real memories must be actively maintained, and meaningful participation in the world requires the ability to manage events as they happen in time and space (4–8). Consequently, autonomous systems must be capable of learning *sequentially* without corrupting previously acquired functions.

For neural networks, intelligent behavior is simply what it means to map inputs to outputs in a way that is accurate or useful, but the space of possible actions and percepts is usually only subject to change retrospectively (9–18). However,

autonomous solutions to problems like catastrophic forgetting require that agents decide for themselves what information is relevant for the tasks they encounter (19–23). This cannot be realized without the freedom to modify elements of morphology, like the number and arrangement of neurons, which specify the inputs that can be detected and the actions that can be performed. To be autonomous, machines must be capable of more than generating accurate predictions; they must, among other things, build and maintain their own sensors and effectors (9, 24–26).

Here we present an algorithm for continual learning that involves the selective recruitment of synapses in a convolutional classifier by a feed-forward regulatory network that observes the same input as the classifier, and which itself undergoes continual change. Regulation is first pre-trained (or “meta-learned”) from an initial state of uniform suppression. This means that no input contains features relevant to the activation of synapses in the classifier. For the system to acquire useful functions the regulator must learn to *disinhibit* the appropriate synapses. Thus, in giving function to initially functionless synapses, the regulator builds sensors for prediction error minimization by establishing “relevance criteria” on inputs not originally specified as relevant (9, 24, 27, 28). In this way, our system becomes more structurally and epistemically autonomous than a traditional neural network, because the information that is detected and optimized by the classifier is expressly a function of regulatory action (Fig.1C,D).

After meta-learning to grow sensors through adaptive disinhibition, the system is trained over long sequences of input sampled from previously unseen datasets, as regulation itself is greedily optimized. As a result, the regulator must learn to recruit, adapt, and maintain previously built sensors for continual learning under foreign conditions. This differs from past efforts to build systems that learn continually, in which meta-learned neural networks are tested on unseen data from *within* the meta-learning distribution (22, 23) rather than unseen data from *outside* the meta-learning distribution (*domain transfer*).

Under domain transfer from Omniglot (29) to ImageNet (30) and CIFAR-100 (31), we find that the regulator facilitates continual learning in the classifier by inducing sparse bursts of scale-free activity in weights that are recycled across tasks, rather than by deploying task-specific modules, as in prior attempts to learn without forgetting (2, 22, 23, 32). By alternating between bursts of activity and suppression the regulator is able to modulate learning in such a way that protects prior knowledge without impeding adaptation to new inputs. Our analysis suggests that an optimal balance of activity and

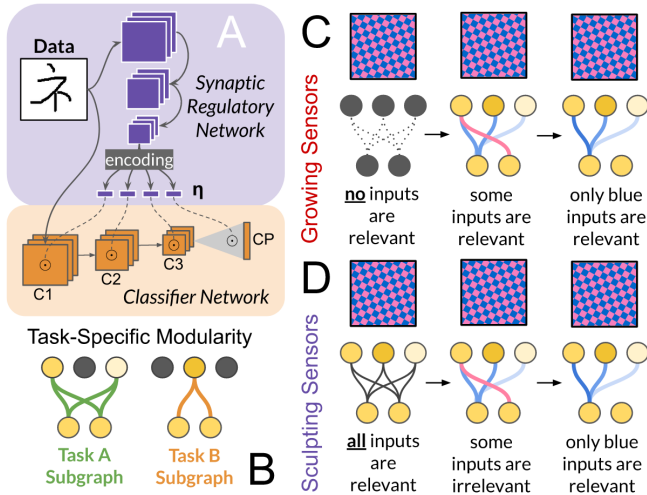


**Fig. 1.** (A) Model architecture for Tuning Synapses via Allostatic Regulation ("TSAR", Materials and Methods). (B) Task-specific modularity helps to overcome forgetting by maintaining disjoint subgraphs that are each recruited to solve a specific task. This may prevent previously learned functions from being overwritten. (C) By initializing meta-learned regulation to be highly suppressant ("Grow", Materials and Methods) we establish a prior on regulation such that no combination of features is relevant to the recruitment of synapses in the classifier. Consequently, the regulator must build sensors by recruiting synapses with initially unspecified functions. In doing so, the regulator develops its own criteria for which weights and inputs are relevant to the supplied objective through its actions alone (9, 24). Conversely, (D) if regulation is initialized to be highly permissive ("Sculpt", Materials and Methods) then *all* inputs are specified as relevant, and meta-learning is the process of making this initial specification more parsimonious. Thus, relevance criteria are autonomously *refined* by sensor sculpting, but autonomously *created* by sensor growth.

suppression is achieved by models set to a specific range of initial meta-learning conditions: when regulation is initialized to be more suppressant or permissive relative to the optimal range, performance drops (often catastrophically).

In particular, the emergence of sparse synaptic bursting depends on meta-learning to *disinhibit* initially suppressed weights (sensor growth), rather than by meta-learning to *suppress* initially disinhibited weights (sensor sculpting). Meta-learned sensor growth is characterized by rapid deregulation, followed by a protracted phase of pruning—culminating in an approximate power law distribution of synaptic recruitment. This mirrors what has been observed for neural development in biological systems, for which initially sparse connectivity gives way to increased synaptic density in early adolescence, and subsequent pruning of excess connections during teenage and adult years (33, 34). We show that meta-learned sensor growth and emergent synaptic bursting enables continual learning under domain transfer even when meta-learning data is reduced to less than 3% of the amount used in prior papers (22, 23).

### Tuning synapses via allostatic regulation.

The system we introduce (Fig.1A, "TSAR") consists of two neural networks: (i) a convolutional classifier network, consisting of three convolutional layers and a linear class prediction layer; and (ii) a feed-forward regulatory network that uses the present input to activate subsets of weights in the classifier for the categorization of that input. In so coupling weights and inputs, the regulator dynamically adjusts the sensors and effectors responsible for generating class predictions. We refer

to regulation of the forward propagation of inputs as synaptic *allostasis* (7) to distinguish it from *homeostatic* modes of regulation, which merely seek to correct unwanted perturbations (2, 35). Regulation of the forward propagation of inputs also indirectly modulates the degree to which regulated weights are updated in light of error, as we demonstrated in prior work on the regulation of neuronal outputs (23). Given the right sequence of regulation, catastrophic forgetting can then be reduced or eliminated by, for example, partitioning the classifier into task-specific modules (Fig.1B). Thus, our model has kinship with fast weight memory systems (15, 16, 36, 37) for which information is dynamically routed through a quickly evolving network by a supervising controller that adapts more slowly. However, we do not explicitly encode operations for maintaining short-term memory, except insofar as previously learned weights are preserved by the regulator.

To maximize control over class predictions, every weight in every layer of the classifier is subject to regulation by multiplicative gating bounded by 0 (completely *inactive*) and 1 (completely *active*). No constraints are placed on when, where, or how much the classifier can learn except those dictated by the regulator in service of prediction error minimization. Consequently, our model belongs to the class of continual learning systems that learn how to learn on the basis of empirical success (14, 38–40), rather than by manually designed rules (2, 32, 41–45).

### Meta-learned sensor construction.

In selecting for the ability to learn without forgetting, we first pre-train TSAR using the Online-aware Meta-Learning algorithm (22), or OML. This is a model-agnostic approach to minimizing predictive interference over an outer loop set of previously observed data following an inner loop of sequential updates (Materials and Methods). Thus, our model must meta-learn how to learn over a sequence of images, such that the corresponding updates do not corrupt the ability to classify prior inputs. This has previously resulted in the acquisition of task-specific modules (Fig.1B) through the optimization of neuronal activations (22, 23). However, task-specific modularity is not required or inevitable; rather, it is a solution that emerged under just one set of conditions through prediction error minimization. Other solutions, under different conditions, may yet be possible.

In addition to configuring our model for the modulation of *synapses* instead of *neurons* (23), we require that the sensors controlled by meta-learned regulation are first "grown" through explicit regulatory action (Fig.1C,D). This is done by initializing meta-learning with regulation that is highly suppressant. In doing so, we are encoding a prior on regulation such that no input is relevant to the recruitment of synapses in the classifier. For performant behavior to emerge, the regulator must increase functional activity relative to the initial meta-learning condition. Catastrophic forgetting is then evaluated under *domain transfer* by training the meta-learned system on extended sequences of previously unseen datasets (Section 5)

### Domain transfer.

Prior studies test the ability of meta-learned neural networks to avoid catastrophic forgetting on previously unseen data sampled from the same domain used for meta-learning, thereby

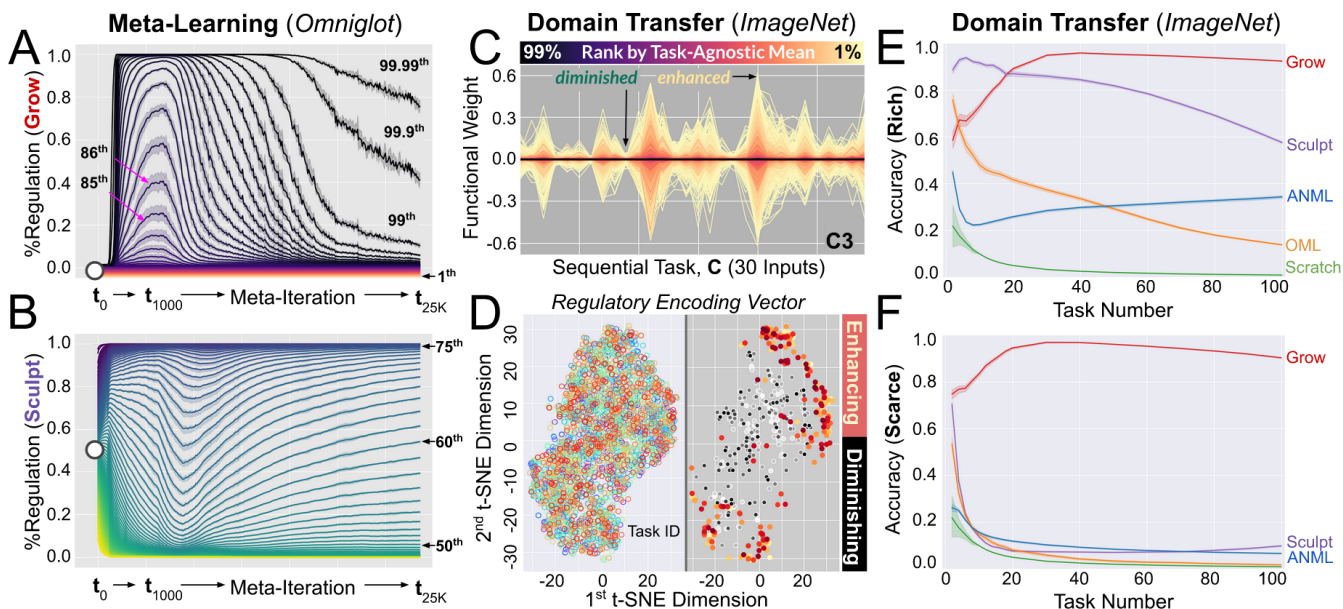


**Fig. 2.** (A) Meta-learned regulation from an initial state of uniform suppression (Grow) results in the rapid deregulation of synapses that are subsequently pruned away as meta-learning proceeds. We plot the  $Q^{th}$  percentile of regulation over time measured across 250 meta-learning classes (3750 total inputs). To highlight transient initial growth, early meta-iterations are plotted with a higher frequency than later meta-iterations. Confidence intervals are computed across runs (lower bound=20th percentile; upper bound=80th percentile). (B) Meta-learned regulation from an initial state of uniform activation (Sculpt) results in a bimodal distribution of regulatory outputs where the modes are centered on near total suppression and activation, respectively. For Sculpt, approximately 50% of all regulatory outputs are suppressant, compared to almost 99% in Grow. Despite initially rapid sculpting, with the 50th percentile decreasing by an average of 0.47 over the first 1000 meta-iterations, regulation at the final meta-iteration is significantly less sparse than in Grow. (C) Regulation in Grow under domain transfer results in collective bursts of *enhanced* and *diminished* activity in the classifier. We plot functional weights in C3 over a randomly sampled task window for a randomly sampled run. Functional weights are synaptic values post-regulatory intervention, and are colored by centile according to ranked mean regulation computed over all domain transfer tasks. (D) Regulator encodings (Fig. 1A, “encoding”) are task-agnostic, while encodings that evoke an enhanced or diminished response are preferentially clustered irrespective of task ID. This may reflect the existence of *meta-stable* states to which the regulator periodically returns on the basis of inputs (46). However, this does not preclude the possibility of task-specific regulatory output (Fig. 3A). Points in the right panel are dimensionally reduced encodings colored according to the ranked mean regulation they produce. Points in the left panel are colored by task identity. Coloring by class identity yields no discernable clusters, and for no run are classes identifiable by their t-SNE projections using K-Nearest Neighbors (SI Appendix, Fig. 5A). This holds not just for regulatory encodings, but also the representations produced by C3 in the classifier (SI Appendix, Fig. 5B). The top 256 encodings ranked by mean consequent regulation are colored on a yellow-red scale (*enhancing*); the bottom 256 encodings ranked by mean regulation are colored on a grey scale (*diminishing*). Dimensional reduction is obtained through a combination of principle component analysis and the t-SNE algorithm (47). (E) ImageNet domain transfer following *data rich* meta-learning (Materials and Methods). Performance curves are generated using 99% bootstrapped confidence intervals ( $n=1000$ ). **Grow**: Mean=92.2% $\pm$  1.1% (SD), **Prune**: Mean=57.5% $\pm$  2.8%, **ANML**: Mean=34.3% $\pm$  6.3% **MRCL**: Mean=13.87% $\pm$  0.729%, **Scratch**: Mean=0.971% $\pm$  0.10%. (F) ImageNet domain transfer following *data scarce* meta-learning (Materials and Methods). **Grow**: Mean=90% $\pm$  2.5% (SD), **Prune**: Mean=9.8% $\pm$  2.9%, **ANML**: Mean=6.6% $\pm$  1.8%, **MRCL**: Mean=1.77% $\pm$  0.57%, **Scratch**: Mean=0.971% $\pm$  0.10%.

limiting the extent to which anything new must be learned (23). Instead, we subject our system to input sequences from entirely new *datasets*. Specifically, we meta-learn on the Omniglot image dataset (29), and test for catastrophic forgetting on input sequences from (truncated) ImageNet (30) and CIFAR-100 (31). By doing so, we subject our system to a process analogous to the transfer of robots from simulation to reality (48), or the introduction of a novel stressor in biology (49). Finally, in an effort to move toward true allostatic regulation (7), in which all parameters are in constant flux, we allow the weights in the regulatory output layer of TSAR to learn along with the synapses they regulate under domain transfer (Fig. 1A, lines emanating from “encoding” vector). This increases susceptibility to forgetting relative to other methods, but allows regulation to adapt to previously unobserved input.

### Virtual analog to the growth of learning.

Existing algorithms for producing sparse neural networks call upon minimally complex subgraphs within large networks for efficient computation (50–53). This is typically achieved by sculpting away synapses that are unnecessary or that interfere with the supplied objective. By contrast, a wealth of literature

attests to the benefits of growing system complexity over time (10–12, 33, 34, 54–56). We hypothesize that one advantage of growth over sculpting is the proximity of the initial state to the least complex (i.e. most sparse) solution, thereby hastening the discovery of “Occam’s Razor” (57). This is particularly important for automating the control of complex systems, as sparse solutions imply the absence of noise and degeneracy, which may amplify causal efficacy (58) and promote the discovery of optimal interventions (59).

For our purposes, regulation can be made to *grow* sensors in the classifier by meta-learning to disinhibit uniformly suppressed synapses, or *sculpted* by meta-learning to suppress uniformly active synapses. We thus obtain Grow and Sculpt regulators by varying the initial strength of regulation to ensure either uniform suppression or activation (Materials and Methods).

All analysis henceforth concerns regulation of the third convolutional layer of the classification network (C3) unless otherwise stated. This is empirically justified by the finding that downstream layers in deep neural networks are the most relevant for understanding performant behavior (62). However, qualitatively identical results were obtained for the regulation



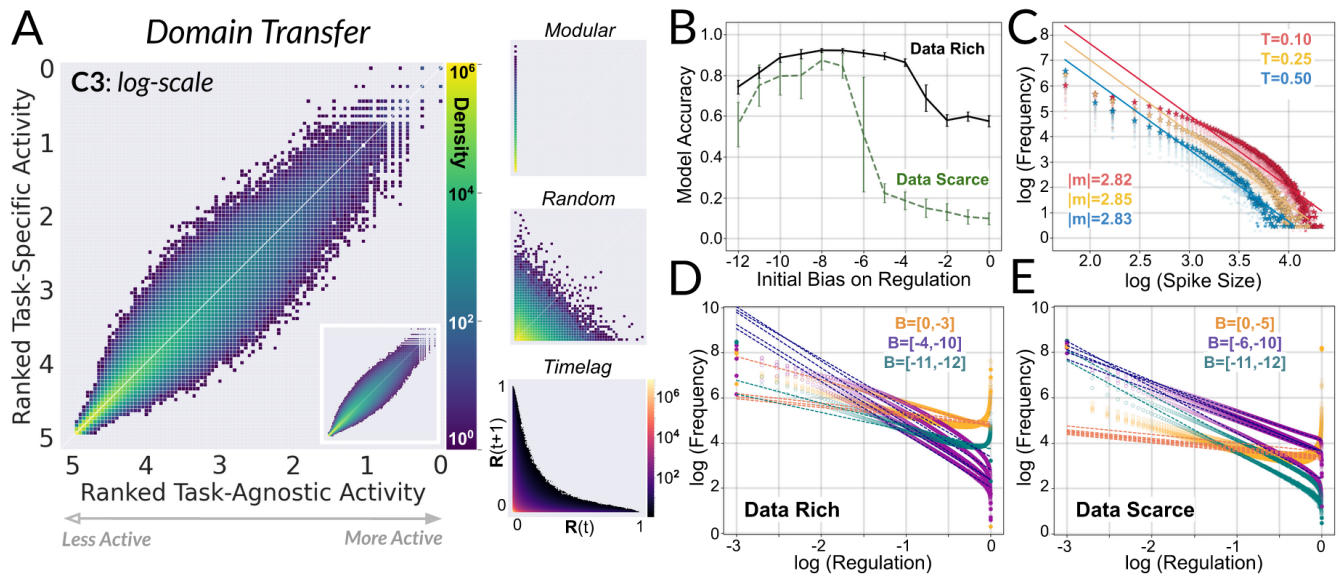


**Fig. 3.** (A) Regulation under domain transfer does not elicit task-specific modularity. Instead, the most active weights on a given task are the most active weights over all tasks, and no synapse drastically changes rank for any individual task (*synaptic recycling*). For each task, regulatory signals are ranked according to their Task-Specific activity (Eq.1) and Task-Agnostic activity (Eq.2). Ranked lists are then transformed to a logarithmic scale (5=least active, 0=most active) and used to fill a two dimensional histogram with 100 bins per dimension (1000 cells in total). The final matrix is filled with data from all 100 tasks and colored by density on a logarithmic scale (60). The inset reports the average over all runs, with cells of density=1 in less than 25% of runs removed, while the main figure reports a single run. See *SI Appendix*, Fig.14 for all individual runs, and Fig.20 for data scarce runs. *Modularity*: as a conceptual aid, we provide a synthetic version of (A) for “perfect” task-specific modularity and Gaussian random regulation. For regulation that is perfectly *Modular*, weights are randomly sorted into 100 disjoint subsets and assigned (i) a random and constant regulatory signal for the task their subset ID corresponds to, and (ii) a value of 0 for every other task, thus producing task-specific modules. For regulation that is *Random*, weights are assigned a Gaussian random regulatory signal for all inputs. *Timelag* (non-synthetic): we observe that highly permissive regulation at time  $t$  is predictive of suppressant regulation at time  $t + 1$ . Thus, synaptic recruitment is highly transient (*synaptic bursting*). Time-lagged regulatory outputs under domain transfer are plotted over all runs by stacking two-dimensional histograms for the 75<sup>th</sup>-99<sup>th</sup> percentile ranked by task-agnostic mean. Centiles ranked lower than 75<sup>th</sup> percentile exhibit even higher transience, if not complete quiescence. We plot the average over the stack of all runs. Outlier cells that have a density less than or equal to 1 post-stacking are masked. Results for individual runs without masking or stacking are presented in (*SI Appendix*, Fig.7). (B) Final performance under domain transfer for different initial meta-learning biases on regulation. For each initial bias not equal to 0 (Sculpt) or -8 (Grow), 10 independent models were procured and evaluated for 40 separate runs. (C) Regulation is calibrated to control the *amount* of sensory processing in the classifier, rather than the task-modular *location* where such processing occurs. Increasingly large spikes, which induce more sensory processing, are correspondingly rare, resulting in an approximate power law distribution. This relationship is observed for all convolutional layers (*SI Appendix*, Fig.7, Fig.8, Fig.9). Each color corresponds to a different threshold for which a synapse is said to burst if it receives regulation above that threshold. Distributions over all runs are plotted with a star, while individual runs are plotted as translucent circles. See *SI Appendix* for analysis of domain transfer to CIFAR-100 for both data rich and data scarce conditions. (D,E) High performance under domain transfer (Fig.3B) is coincident with particular patterns of regulation, in which highly suppressant regulation dominates and increasingly permissive regulation is correspondingly rare. These patterns only emerge for a certain range of initial meta-learning biases on regulatory output. We believe this reflects a purposive balance of permission and suppression that is analogous to the balance of order and disorder in edge of chaos criticality (61). For data rich (D) and data scarce (E) meta-learning, good regulators (*purple*) exhibit an approximate power law distribution under domain transfer within a specific range of scaling factors. Comparatively worse regulators (*orange* and *teal*) fall outside of this range (more suppressant) or exhibit super-linear distributions (more permissive). We present the highest performing runs for each model. All runs for all models are shown in *SI Appendix*. Initial biases equal to -9 and -10 for data rich meta-learning fall in the purple cohort of good regulators, but are omitted from (D) for clarity (see *SI Appendix*, Fig.24).

of upstream convolutional layers (*SI Appendix*).

We find that meta-learning to grow sensors from an initial state of uniform suppression produces highly sparse regulation that follows from the gradual pruning of synapses whose activity rapidly increases at the start of meta-learning (Fig.2A, “Grow”). This process resembles synaptic growth and pruning in developing neurobiological systems (33), and may reflect a transition from exploration to exploitation (34). Meanwhile, Sculpt meta-learns to suppress synapses that are initially active, but does not produce comparably sparse regulatory output—emitting regulation that is either highly permissive or suppressant (Fig.2B).

However, the logic of meta-learned regulation in either case is not apparent from these facts alone, nor is it obvious whether sensors that have been grown or sculpted by meta-learning can be recruited to learn continually under domain transfer. In the next section we show that meta-learning to grow sensors through purposive deregulation militates against forgetting, while meta-learning to sculpt sensors through suppression

does not. After presenting empirical results, we investigate the mechanisms by which forgetting is overcome by meta-learned regulation in Grow (Section 6, Section 7, Section 8).

## Performance.

Fig.2E reports classification accuracy under domain transfer to ImageNet for models trained sequentially over 100 randomly ordered classes across 250 trials (Materials and Methods). Each class contains 30 randomly sampled images from a set of 600 possible images, yielding a total of 3,000 sequential gradient updates per trial. Accuracy is measured as the degree to which prior inputs can be recalled. This captures the phenomenon of forgetting by quantifying how much of what was actually learned is retained over time (22).

We find that Grow adapts to the new domain without significant loss in performance as new tasks are encountered, while competing methods adapt sub-optimally or forget catastrophically. At the same time, validation accuracy under domain transfer is low for all models (*SI Appendix*, Fig.5D). This can



be attributed to the inherent difficulty of generalization in a foreign domain from few examples learned sequentially. Nevertheless, when trained on a 600-task sequence (*SI Appendix, Fig.5F*) of previously unobserved data sampled from the same domain used for meta-learning, as per (23), Grow remembers prior inputs with almost perfect accuracy (train=95.2%) and obtains validation accuracy (test=43.8%) that is second only to the current state of the art on this problem (ANML, train=89%, test=65%) which owes its high performance to learning being disabled in all but its final layer (23). Grow is competitive with ANML on this problem despite (i) having many more degrees of freedom and, therefore, greater susceptibility to forgetting; and (ii) using a classifier with less than half the capacity (*Materials and Methods*). By comparison, Sculpt achieves an average of just 15.1% training accuracy and 2.6% testing accuracy on this 600 task problem (*SI Appendix, Fig.5F*).

To evaluate robustness against the degradation of available meta-learning data, we prepared models identical to those presented in Fig.2E but reduced the size of the meta-learning dataset to less than 3% of the original condition (*Materials and Methods*). We find that the performance of Grow modestly declines relative to the data rich condition, while the other algorithms suffer significant loss in accuracy. Notably, data scarce meta-learning in Grow produces a model that outperforms all other *data rich* models under domain transfer. Similar results obtain for evaluation over CIFAR-100 with minor variations in accuracy (*SI Appendix, Fig.5*). In the next section, we interrogate the means by which TSAR is able to learn continually under domain transfer.

### Task-specific modularity.

Past efforts to solve catastrophic forgetting have relied on task-specific modules for conditionally modifying disjoint sets of weights (2, 22, 23, 32). To determine whether regulation in TSAR is calibrated for such task-specific modularity (Fig.1B), we reason that task-specific modules should be characterized by heightened synaptic activity within a given task but reduced activity for all other tasks. Task-Specific activity for synapse  $i$  in layer  $\ell$  is computed as the average regulatory signal governing that synapse,  $\eta_i^\ell$ , over all  $K$  instances of a given task,  $C$  (Eq.1). Meanwhile, Task-Agnostic activity is computed as the average Task-Specific activity over all tasks not equal to  $C$  (Eq.2). In accordance with prior work (50, 51), we take activity to be a proxy for salience, and therefore regard ranked activity as ordered importance. For Grow, regulation is approximately scale-free (Fig.3D,E); as such, we are concerned with logarithmic rank (60). Task-specific modularity, or its absence, can then be visualized by plotting ranked Task-Specific activity against ranked Task-Agnostic activity for each task under domain transfer (Fig.3A).

$$\text{Task-Specific Activity} = \frac{1}{K} \sum_{k=0}^K \eta_i^\ell(C_k) \quad [1]$$

$$\text{Task-Agnostic Activity} = \frac{1}{T-1} \sum_{t \neq C} \frac{1}{K} \sum_{k=0}^K \eta_i^\ell(t_k) \quad [2]$$

We find that the synapses which are most active on a given task are among the most active overall (*synaptic recycling*).

Indeed, the majority of weights rank similarly over all tasks as they do for any individual task. Finally, we do not find that any synapse which ranks high for any given task ranks low for all other tasks. Thus, we do not see evidence for task-specific *modularity* in the output of the regulatory network.

### Synaptic bursting.

In the absence of task-specific modularity, we find that synapses are conditionally recruited for task-agnostic bursting (Fig.2C,D, Fig.3A,C, “Timelag”, *SI Appendix*). This is characterized by the onset of highly transient activity in response to particular *images* rather than particular *tasks* (Fig.3A). The simultaneous bursting of multiple synapses generates large spikes of activity in weights that are otherwise suppressed. This produces waves of enhanced and diminished sensory processing in the classifier (Fig.2C). Furthermore, we find that the distribution of performant regulation under domain transfer follows an approximate power law (Fig.3B,D,E), and that the *number* of synapses that burst during enhanced processing is also approximately power law distributed (Fig.3C). In both cases, the occurrence of increasingly high magnitude events is correspondingly rare. The coincidence of multiple power laws is characteristic of critical phenomena (63), and analysis of both regulatory output (Fig.3D,E) and model performance (Fig.3B) for different initial meta-learning biases on regulation suggests a critical range in which performance is optimized.

Criticality has previously been implicated in optimal information propagation (64, 65) and storage (66, 67) in artificial networks, and is believed to play a role in the adaptive behavior of living systems (68). It has also been associated with the emergence of scale-free avalanches (61, 69, 70) in systems which may or may not be situated at the edge of chaos (71). We hypothesize that the range of initial meta-learning biases on regulation that produce optimal performance under domain transfer corresponds to a critical region in which activity and suppression are appropriately balanced. Thus, regulation is calibrated to control the *amount* of processing in classifier, by transiently activating subsets of weights that are recycled across tasks, rather than the task-modular *location* where such processing occurs. In this way, our model resolves the tension at the heart of continual learning, in which too much activity facilitates adaptation but causes forgetting, while too little activity preserves extant functions at the expense of future adaptation. We investigate the extent to which performance under domain transfer is impacted by a balance of enhanced and diminished perception in the section that follows.

### Enhanced and diminished perception.

Analysis of the shared vector from which all regulation is produced (Fig.1A, “encoding”) reveals that images are represented by the regulator in a way that is related to their consequent level of overall recruitment rather than by task identity (Fig.2D). Given that images can be so classified by the mean regulation they produce, we can isolate the effects of enhanced and diminished processing on model performance by training on sequences of exclusively enhancing or diminishing images. This is possible because the *mean* regulatory output for a given image is virtually identical when learning in the regulatory output layer is enabled under domain transfer relative to when it is disabled (*SI Appendix, Fig.5C*). *Enhancing*

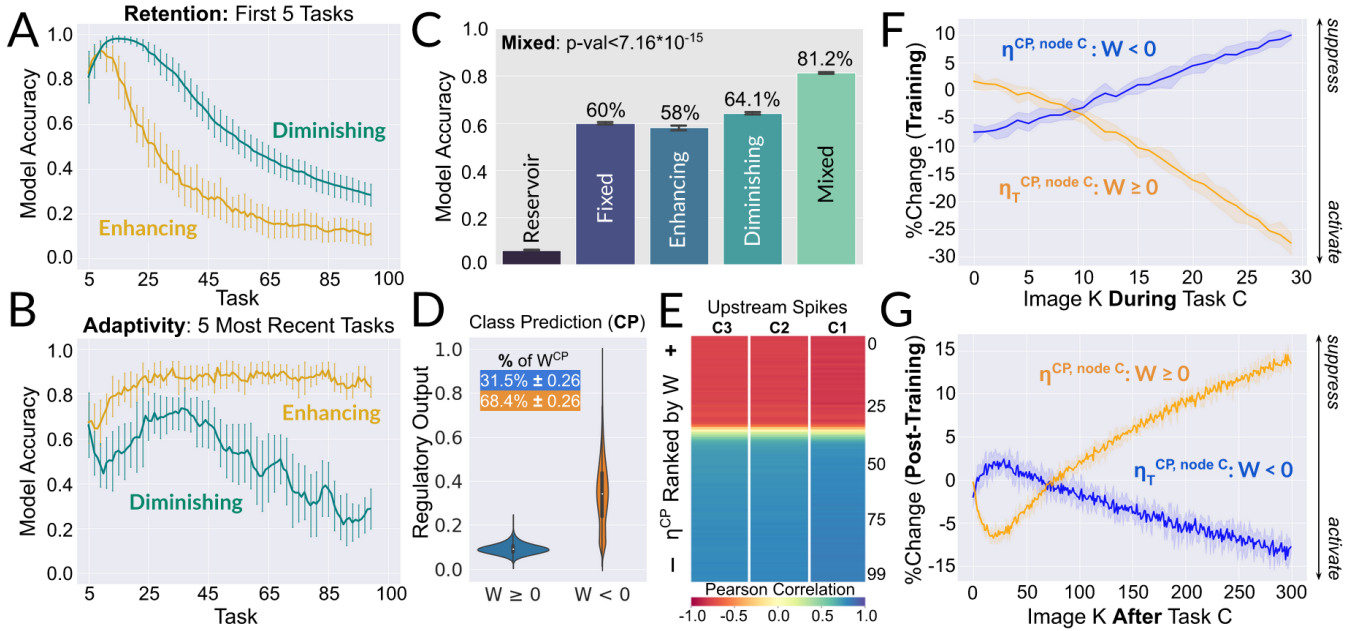


**Fig. 4.** (A) The effect of enhanced perception on past inputs is to corrupt previously acquired functions, while the effect of diminished perception is to guard against corruption. (B) The effect of enhanced perception on recent inputs is to facilitate adaptation, while the effect of diminished perception is to hinder adaptation. (C) Performance is highest when a balance of enhanced and diminished perception is induced. For “Mixed”, the images that comprise a given task are randomly sampled from the “Enhancing” and “Diminishing” datasets with equal probability. “Fixed” refers to the treatment where regulatory output to C1, C2, and C3 is not subject to optimization under domain transfer, showing that performance is not simply a result of fine-tuning the class prediction layer. “Reservoir” reports model performance for randomly initialized regulation with no meta-learning. (D) In the class prediction layer, positive weights are regulated differently than negative weights. This was not observed for convolutional layers. We also find that training the CP layer under domain transfer results in more than twice as many negative weights as positive weights. (E) Positive weights in CP are safely updated when sensory processing in upstream layers is most diminished. During enhanced perception, negative weights are *suppressed* and positive weights are *activated*. During diminished perception, positive weights are *activated* and negative weights are *suppressed*. This is shown by the correlation of upstream spikes with the regulation of negative weights in CP, and the inverse correlation of upstream spikes with the regulation of positive weights in CP. Upstream spikes are defined as the mean regulation for the top 10% of weights in upstream layers ranked by mean regulation over all images. Pearson correlation is computed over domain transfer with respect to (i) the first difference for the mean regulation governing weights in CP ranked by weight value and grouped centile; and (ii) the first difference for upstream spikes. (F) Contextual information encoded in positive weights is accumulated during training. Over the course of a given task, negative weights innervating the correct class prediction node are increasingly *suppressed* while positive weights innervating the correct class node are increasingly *activated*. Percent change is computed over 20 random runs with respect to mean regulation emitted at the final step of the immediately prior task. (G) Contextual information encoded in positive weights is protected when exposed to new tasks. Following a brief refractory period, in which the trends observed in (F) persist over future inputs, positive weights innervating the class prediction nodes of previously seen tasks are increasingly *suppressed* while the negative weights innervating the class prediction nodes of previously seen tasks are *activated*. Percent change is computed over 20 random runs with respect to mean regulation emitted at the final step of that task.

and *Diminishing* datasets are then composed of the top 30 and bottom 30 images per task ranked by mean regulatory output with respect to the model under consideration (out of a possible 600 images per task).

When Grow is trained on the Enhancing and Diminishing datasets performance drops to  $58.05\% \pm 3.8\%$  (SD) and  $64.1\% \pm 2\%$ , respectively (Fig.4C, “Diminishing”, “Enhancing”). However, when the system is trained on even mixtures of enhancing and diminishing images, performance increases relative to both conditions,  $81.2\% \pm 1.4\%$  (Fig.4C, “Mixed”: p-value  $< 7.16 \times 10^{-15}$ , Mann-Whitney U). By visualizing changes in accuracy over time (Fig.4A,B), we find that training on enhancing images degrades retention of past performance but promotes adaptation to new inputs. Conversely, past performance is protected when training on diminishing images, while new inputs become harder to learn. These results suggest that our model is able to adapt to novel conditions without corrupting prior functions by maintaining a balance of enhanced and diminished perception (72).

Finally, we observe that regulation of the class prediction layer (CP) produces markedly different distributions for positive and negative weights (Fig.4D). In particular, positive

weights in CP are held at relatively low values with infrequent variation, while negative weights in CP exhibit comparatively high variation around a larger mean value. At the same time, positive and negative weights are differentially correlated with upstream activity, such that negative weights are enhanced and diminished in synchrony with upstream weights, but positive weights are diminished during upstream *enhancement* and enhanced during upstream *diminishment* (Fig.4E).

In light of this, we hypothesize that the coordination of enhanced and diminished perception with downstream regulation functions as a visual sampling mechanism (72, 73) that arises opportunistically under domain transfer. For biological systems engaged in such sampling procedures, visual attention alternates between enhanced and diminished states that respectively engage “sampling” and “shifting” mechanisms. While sampling, sensory processing is enhanced while motor and attentional shifts are suppressed. Conversely, shifting states are associated with attenuated perceptual activity, which provides the opportunity to safely update attention, motoric output, and other important variables.

In our system, the way in which positive weights in CP are regulated suggests the long-term storage of contextual

information obtained by protected change in the underlying set of weights (Fig.4F,G), which are most active when sensory processing is most diminished (Fig.4E). On the other hand, the synchronization of negative weights in CP with bursts of activity in upstream layers is consistent with the joint sampling of inputs and class predictions (Fig.4A). However, we find that optimizing the regulation of CP under domain transfer is not, on its own, sufficient to achieve high performance: when the layers that produce regulation for upstream convolutions is fixed, but regulation of CP is made labile, performance drops relative to the condition where regulatory output for all layers is labile (Fig.4C, “Fixed”).

## Discussion.

Among the factors responsible for the resilience of living systems is the ability to impose meaning on the world through the negotiation of bodily form and function (9, 24, 25, 74–77). Consequently, action and perception are not defined by information communicated over anatomically fixed, yet tunable, channels (26, 78, 79). Rather the means by which information is made and communicated are themselves subject to purposive modification. Thus, encoded in the very structure of living systems is that which counts as meaningful (8, 74, 80–82). By contrast, machine learning algorithms typically undergo morphological change only in light of error (51), or by random mutation (14), which renders them partially autonomous systems for error *correction* rather than error *prevention* (7, 35).

In the preceding sections we presented a machine learning algorithm for dynamically regulating synapses in a convolutional neural network for continual learning over long sequences of previously unseen datasets. We demonstrated that effective regulation under domain transfer depends on a degree of structural and epistemic autonomy (9, 24) resulting from the adaptive construction of sensors in the classifier. This occurs by meta-learning to disinhibit synapses initialized to a state of uniform suppression, leading to the autonomous construction of relevance criteria on inputs.

Under domain transfer, we find that regulation does not elicit task-specific modularity, but instead induces sparse bursts of activity in weights that are recycled across tasks. Sparse synaptic bursting, whose emergence is sensitive to initial meta-learning conditions, is found to be approximately power law distributed in both raw output (Fig.3D) and in the number of synapses recruited to burst (Fig.3C). We hypothesize that such sparse synaptic bursting induces an optimal balance of enhanced and diminished processing in the classifier, which allows adaptation to new inputs without corrupting extant functions. This addresses the core dilemma posed by sequential learning: too much change causes forgetting, while too little change induces brittleness. The discovery of sparse synaptic bursting for maintaining a balance of opposing states may be fruitfully analogized to the behavior of biological systems across various niches, scales, and modalities (68, 72, 83–87). Finally, we presented evidence that contextual information encoded in the positive weights of the class prediction layer is safely obtained during occasions of diminished perception, and subsequently protected under contextual shifts (Fig.4F,G).

Our findings may be of immediate use in the creation and control of programs for computer vision, reinforcement learning, and robotics. Additionally, our system may be helpful in understanding how information is stored and transmitted in

biological systems marked by perpetual change, stochasticity, opportunism, and multiple functionality (79, 84, 88–90). More abstractly, we believe our work contributes to a growing literature that rejects the supremacy of fixed and fragile automata (91–94). As advances in biology continue to undermine the view that life’s constituent parts are little more than (20th century) machines (26, 79), our technologies should likewise be reconfigured for perpetual and collective modification in response to individual and social preference. The ability to learn new information without forgetting will be critical in the transition to such increasingly protean technology (95).

## Materials and Methods

**Meta-Learning Algorithm.** We use the model-agnostic Online Meta-Learning algorithm (22) for learning how to learn over the background partition of the Omniglot image dataset (29). This dataset contains 963 hand-written character classes from various human alphabets. Each character class contains 20 unique instances (15 for training; 5 for testing). All images are resized to 3x28x28 (channels, height, width). A single meta-iteration consists of (i) an inner loop of sequential training on a 20 image batch sampled with replacement from the set of 15 meta-training images for a single character class  $c_m \sim \mathcal{C}$ ; and (ii) an outer loop that evaluates performance retention on a random batch of 84 images sampled from the set of meta-testing images over all classes. Of the 84 images in the performance retention set, 20 are sampled with replacement from the set of 5 meta-testing images from the inner loop class,  $c_m$ , while the other 64 images are randomly sampled from the remaining set of 962 character classes.

Prediction error on the performance retention set at the end of the inner loop sequence for network  $\Theta_K^m$  is back-propagated through the entire model to update the weights used at the beginning of the inner loop sequence,  $\Theta_0^m$ . These new initial weights are then carried over into the next meta-iteration,  $\Theta_0^{m+1} \propto \Theta_0^m + \text{update}$ . Learning within each inner loop is discarded: only the initial weights, or the conditions under which inner loop learning occurs, are optimized over the outer loop (39). Successful meta-learners will have learned to learn over the inner loop without interfering with the classification of outer loop images, thus directly optimizing for the ability to learn without forgetting or interference (22).

Treatments presented in this paper differ both in their architecture, and in which layers are changeable during inner loop meta-learning. Consequently, we make no claims as to the *inherent* superiority of one model over another. Each treatment, having 25 independent models, was meta-learned for 25,000 meta-iterations on a single NVIDIA Tesla V100 GPU. For more details regarding the meta-learning protocol see (22, 23, 39).

All models will be made available for download. If the reader would like to replicate or extend this work, but lacks the necessary resources, requests for computation can be addressed to the primary author.

**Data Rich/Scarce Meta-Learning.** Data rich meta-learning uses the full background set of Omniglot images (963 character classes) for the OML protocol. The data scarce condition instead uses less than 3% of the meta-learning data used in the data rich condition (25 randomly sampled character classes).

**Domain Transfer.** After executing the meta-learning protocol, each model is trained over a sequence of 100 classes from a previously unobserved dataset (ImageNet or CIFAR-100). Classes contain 600 total images, from which 30 are randomly sampled without replacement for each class. This translates to 3000 (100\*30) sequential iterations of gradient descent. All images are resized to 3x28x28 (channels, height, width). Every run uses a different random seed, a randomized class order, and a random batch of 30 images per class. We applied a grid search over learning rates, and selected the highest performing setting over all subsequent runs.



**OML.** See (22, 23) for more details regarding theoretical motivation and network architecture. No changes were made to the meta-learning protocol, except to implement a post-publication correction for computing second-order gradients. The OML treatment, which is distinct from the OML *protocol*, consists of two neural networks: a representation learning network (RLN) composed of five convolutional layers, and a prediction learning network (PLN) composed of two linear layers that takes as input the output of the RLN. During meta-learning, the RLN is updated over the outer loop, while the PLN is updated in both the inner and outer loops. Under domain transfer, the RLN is fixed over the course of training, while the PLN is fully changeable. Prior to domain transfer, the class prediction layer (CP) of the PLN is randomly reset as per (22). This algorithm depends on the RLN meta-learning to produce sparse-disjoint inputs to the PLN for effective continual learning. Consequently, this algorithm avoids catastrophic forgetting by virtue of task-specific modularity (Fig.1B).

**TSAR.** TSAR (Fig.1A) consists of two neural networks: a regulatory network, and a classifier network. The regulatory network consists of (i) a perception module; and (ii) a regulatory output layer. The regulatory perception module contains 3 convolutional layers, each containing 192 channels (window size=(3,3), stride=1, padding=0). The output of each convolutional layer is processed with instance normalization and then passed through a ReLU non-linear activation function. Max-pooling layers (stride=2, kernel size=2) are placed after the first two convolutional layers of the perception module to create an input encoding layer of size 1728 from which all regulatory output is generated (Fig.1A).

The regulatory output layer consists of four weight matrices, each of which produces a set of regulatory outputs that govern a unique layer in the classification network. Raw outputs from the regulatory output layer are processed using a sigmoidal activation. Processed outputs then modulate synapses in the classifier via multiplicative gating ( $\eta^\ell \odot W^\ell$ , for layer  $\ell$  in the classifier).

The classification network is made up of three convolutional layers (112 channels, window size=(3,3), stride=1, padding=0) and a linear output, or class prediction, layer (CP). Max-pooling layers (stride=2, kernel size=2) are placed after each convolutional layer and are followed by instance normalization and a ReLU non-linearity. Class predictions are computed with a softmax function applied to the raw output of the modulated CP layer. During meta-learning, the regulatory network is fixed during inner loop learning, but the prediction network is changeable. All parameters receive updates in the outer loop.

Under domain transfer, all layers in the prediction network are changeable. The regulatory output layer is also changeable. Only the convolutional layers of the regulatory network are fixed. As with OML, the CP layer (and the regulatory output that flows to this layer) is reset before domain transfer.

**Grow and Sculpt.** For *Grow*, all biases in the regulatory output layer are initialized to a value of -8 before executing the meta-learning protocol. Due to the sigmoidal activation, this results in initially high levels of suppression. For *Sculpt*, all biases in the regulatory output layer are initialized to the standard bias of 0 before executing the meta-learning protocol. Thus, all things being equal, all synapses in the classification network of *Sculpt* begin meta-learning with their functional values approximately halved ( $\text{sigmoid}(0.0)=0.5$ ). Under domain transfer, regulatory output to CP is reset with a bias of -2 for *Grow*. This value was obtained using a grid search over biases and learning rates on domain transfer accuracy. Regulatory output to CP for *Sculpt* is reset with a bias of 0. We found the final performance of *Sculpt* did not significantly change with increasingly negative re-initializations of the bias term on regulatory output under domain transfer.

**ANML.** ANML (23) consists of two neural networks: a regulatory network, and a classifier network. The regulatory network has the same architecture used for TSAR, except it produces a single output vector of size 2304 which is transformed with a sigmoidal activation. The classifier network in ANML differs from TSAR in having 256 channels per convolutional layer, and in having the maxpooling operation at the penultimate layer of the classifier removed. This results in the penultimate layer of the classifier producing a large

vector,  $R$ , of size 2304 that feeds into the class prediction layer. Regulatory intervention by multiplicative gating occurs at this large vector ( $R \odot \eta$ ) before it is used to make a class prediction. This algorithm depends on meta-learning to produce sparse-disjoint inputs to the class prediction layer (post-regulatory intervention) for effective continual learning. See (23) for more details regarding theoretical motivation. Consequently, this algorithm avoids catastrophic forgetting by virtue of task-specific modularity (Fig.1B).

**Scratch.** This treatment uses the classification network architecture described for TSAR, but with regulation disabled. Scratch is subject to domain transfer training from a random initialization with no meta-learning.

**ACKNOWLEDGMENTS.** This work is supported in part by the DARPA Lifelong Learning Machines award HR0011-18-2-0018. We'd like to thank Josh C. Bongard, Sam Kriegman, and Kate Nolfi for discussion and proofreading. Computations were performed on the Vermont Advanced Computing, supported in part by NSF award No.OAC-1827314. We also recognize the Vermont Complex Systems Center for assistance, encouragement, and feedback, particularly Lapo Frati and Colin Van Oort.

1. MR French, Catastrophic forgetting in connectionist networks. *Trends Cogn. Sci.* **3**, 128–135 (1999).
2. J Kirkpatrick, et al., Overcoming catastrophic forgetting in neural networks. *Proc. Natl. Acad. Sci.* **114**, 3521–3526 (2017).
3. D Rolnick, A Ahuja, J Schwarz, T Lillicrap, G Wayne, Experience replay for continual learning in *Advances in Neural Information Processing Systems*, eds. H Wallach, et al. (Curran Associates, Inc.), Vol. 32, (2019).
4. F Varela, H Maturana, R Uribe, Autopoiesis: The organization of living systems, its characterization and a model. *Biosystems* **5**, 187–196 (1974).
5. SJ Cooper, From claudes bernard to walter cannon. emergence of the concept of homeostasis. *Appetite* **51**, 419–427 (2008).
6. D Bullock, Adaptive neural models of queuing and timing in fluent action. *Trends Cogn. Sci.* **8**, 426–433 (2004).
7. J Schulkin, P Sterling, Allostasis: A brain-centered, predictive mode of physiological regulation. *Trends Neurosci.* **42**, 740–752 (2019).
8. K Man, A Damasio, Homeostasis and soft robotics in the design of feeling machines. *Nat. Mach. Intell.* **1**, 446–452 (2019).
9. P Cariani, To evolve an ear. epistemological implications of gordon pask's electrochemical devices. *Syst. Res.* **10**, 19–33 (2007).
10. J Bongard, Morphological change in machines accelerates the evolution of robust behavior. *Proc. Natl. Acad. Sci.* **108**, 1234–1239 (2011).
11. A Bernatskiy, JC Bongard, Exploiting the relationship between structural modularity and sparsity for faster network evolution in *Proceedings of the Companion Publication of the 2015 Annual Conference on Genetic and Evolutionary Computation*. (ACM), (2015).
12. G Raghavan, M Thomson, Neural networks grown and self-organized by noise in *Advances in Neural Information Processing Systems*, eds. H Wallach, et al. (Curran Associates, Inc.), Vol. 32, (2019).
13. Y Jaafra, J Luc Laurent, A Deruyver, M Saber Naceur, Reinforcement learning for neural architecture search: A review. *Image Vis. Comput.* **89**, 57–66 (2019).
14. KO Stanley, R Miikkilainen, Evolving neural networks through augmenting topologies. *Evol. Comput.* **10**, 99–127 (2002).
15. J Schmidhuber, Learning to control fast-weight memories: An alternative to dynamic recurrent networks. *Neural Comput.* **4**, 131–139 (1992).
16. J Ba, GE Hinton, V Mnih, JZ Leibo, C Ionescu, Using fast weights to attend to the recent past in *Advances in Neural Information Processing Systems*, eds. D Lee, M Sugiyama, U Luxburg, I Guyon, R Garnett. (Curran Associates, Inc.), Vol. 29, (2016).
17. K Greff, S van Steenkiste, J Schmidhuber, On the binding problem in artificial neural networks. *CoRR abs/2012.05208* (2020).
18. I Schlag, K Irie, J Schmidhuber, Linear transformers are secretly fast weight memory systems. *CoRR abs/2102.11174* (2021).
19. AJ Bell, TJ Sejnowski, An information-maximization approach to blind separation and blind deconvolution. *Neural Comput.* **7**, 1129–1159 (1995).
20. K Fukushima, Neocognitron: A hierarchical neural network capable of visual pattern recognition. *Neural Networks* **1**, 119–130 (1988).
21. RL Fry, The engineering of cybernetic systems in *AIP Conference Proceedings*. (AIP), (2002).
22. K Javed, M White, Meta-learning representations for continual learning in *Advances in Neural Information Processing Systems*, eds. H Wallach, et al. (Curran Associates, Inc.), Vol. 32, pp. 1820–1830 (2019).
23. S Beaulieu, et al., Learning to continually learn in *Proceedings of the 24th European Conference on Artificial Intelligence*. (2020).
24. G Pask, The simulation of learning and decision-making behavior in *Aspects of the Theory of Artificial Intelligence*. (Springer US), pp. 165–210 (1962).
25. M Pharoah, Causation and information: Where is biological meaning to be found? *Biosemiotics* **13**, 309–326 (2020).
26. J Bongard, M Levin, Living things are not (20th century) machines: Updating mechanism metaphors in light of the modern science of machine behavior. *Front. Ecol. Evol.* **9** (2021).
27. JM Mandler, How to build a baby: II. conceptual primitives. *Psychol. Rev.* **99**, 587–604 (1992).

28. J Köber, B Mohler, J Peters, Learning perceptual coupling for motor primitives in *2008 IEEE/RSJ International Conference on Intelligent Robots and Systems*. pp. 834–839 (2008).
29. BM Lake, R Salakhutdinov, JB Tenenbaum, Human-level concept learning through probabilistic program induction. *Science* **350**, 1332–1338 (2015).
30. O Russakovsky, et al., ImageNet large scale visual recognition challenge. *Int. J. Comput. Vis.* **115**, 211–252 (2015).
31. A Krizhevsky, G Hinton, Learning multiple layers of features from tiny images. (2009).
32. KO Ellefsen, JB Mouret, J Clune, Neural modularity helps organisms evolve to learn new skills without forgetting old skills. *PLoS Comput. Biol.* **11**, e1004128 (2015).
33. U Nenislyte, CT Gross, Errant gardeners: glial-cell-dependent synaptic pruning and neurodevelopmental disorders. *Nat. Rev. Neurosci.* **18**, 658–670 (2017).
34. A Gopnik, Childhood as a solution to explore–exploit tensions. *Philos. Transactions Royal Soc. B: Biol. Sci.* **375**, 20190502 (2020).
35. RC Conant, WR Ashby, Every good regulator of a system must be a model of that system. *Int. J. Syst. Sci.* **1**, 89–97 (1970).
36. WR Ashby, *Design for a brain: The origin of adaptive behaviour (2nd ed. rev.)*. (Chapman & Hall), (1960).
37. B Tsuda, KM Tye, HT Siegelmann, TJ Sejnowski, A modeling framework for adaptive lifelong learning with transfer and savings through gating in the prefrontal cortex. *Proc. Natl. Acad. Sci.* **117**, 29872–29882 (2020).
38. F Zenke, B Poole, S Ganguli, Continual learning through synaptic intelligence in *Proceedings of the 34th International Conference on Machine Learning*, Proceedings of Machine Learning Research, eds. D Precup, YW Teh. (PMLR, International Convention Centre, Sydney, Australia), Vol. 70, pp. 3987–3995 (2017).
39. C Finn, P Abbeel, S Levine, Model-agnostic meta-learning for fast adaptation of deep networks in *Proceedings of the 34th International Conference on Machine Learning*, Proceedings of Machine Learning Research, eds. D Precup, YW Teh. (PMLR, International Convention Centre, Sydney, Australia), Vol. 70, pp. 1126–1135 (2017).
40. H Pham, M Guan, B Zoph, Q Le, J Dean, Efficient neural architecture search via parameters sharing in *Proceedings of the 35th International Conference on Machine Learning*, Proceedings of Machine Learning Research, eds. J Dy, A Krause. (PMLR, Stockholmssmässan, Stockholm Sweden), Vol. 80, pp. 4095–4104 (2018).
41. D Isele, A Cosgun, Selective experience replay for lifelong learning. *Proc. AAAI Conf. on Artif. Intell.* **32** (2018).
42. C Fernando, et al., Pathnet: Evolution channels gradient descent in super neural networks. *ArXiv abs/1701.08734* (2017).
43. MR French, Semi-distributed representations and catastrophic forgetting in connectionist networks. *Connect. Sci.* **4**, 365–377 (1992).
44. X Li, Y Grandvalet, F Davoine, Explicit inductive bias for transfer learning with convolutional networks in *Proceedings of the 35th International Conference on Machine Learning*, Proceedings of Machine Learning Research, eds. J Dy, A Krause. (PMLR, Stockholmssmässan, Stockholm Sweden), Vol. 80, pp. 2825–2834 (2018).
45. J Zhang, et al., Top-down neural attention by excitation backprop. *Int. J. Comput. Vis.* **126**, 1084–1102 (2017).
46. C Haldeman, JM Beggs, Critical branching captures activity in living neural networks and maximizes the number of metastable states. *Phys. Rev. Lett.* **94** (2005).
47. L van der Maaten, G Hinton, Visualizing data using t-sne. *J. Mach. Learn. Res.* **9**, 2579–2605 (2008).
48. JB Mouret, K Chatziligeroudis, 20 years of reality gap in *Proceedings of the Genetic and Evolutionary Computation Conference Companion*. (ACM), (2017).
49. M Emmons-Bell, et al., Regenerative adaptation to electrochemical perturbation in planaria: A molecular analysis of physiological plasticity. *iScience* **22**, 147–165 (2019).
50. Y LeCun, JS Denker, SA Solla, Optimal brain damage in *Advances in Neural Information Processing Systems*. (Morgan Kaufmann), pp. 598–605 (1990).
51. H Tanaka, D Kunin, DLK Yamins, S Ganguli, Pruning neural networks without any data by iteratively conserving synaptic flow. *CoRR abs/2006.05467* (2020).
52. U Evci, YA Ioannou, C Keskin, Y Dauphin, Gradient flow in sparse neural networks and how lottery tickets win (2020).
53. Y Bengio, N Léonard, AC Courville, Estimating or propagating gradients through stochastic neurons for conditional computation. *ArXiv abs/1308.3432* (2013).
54. SA Kauffman, Autocatalytic sets of proteins. *J. Theor. Biol.* **119**, 1–24 (1986).
55. DJ Watts, SH Strogatz, Collective dynamics of ‘small-world’ networks. *Nature* **393**, 440–442 (1998).
56. O Sports, DR Chialvo, M Kaiser, CC Hilgetag, Organization, development and function of complex brain networks. *Trends Cogn. Sci.* **8**, 418–425 (2004).
57. A Baker, Simplicity in *The Stanford Encyclopedia of Philosophy*, ed. EN Zalta. (Metaphysics Research Lab, Stanford University), Winter 2016 edition, (2016).
58. EP Hoel, L Albantakis, G Tononi, Quantifying causal emergence shows that macro can beat micro. *Proc. Natl. Acad. Sci.* **110**, 19790–19795 (2013).
59. J Pearl, *Causality: Models, Reasoning and Inference*. (Cambridge University Press, USA), 2nd edition, (2009).
60. PS Dodds, et al., Allotaxonomy and rank-turbulence divergence: A universal instrument for comparing complex systems (2020).
61. SA Kauffman, S Johnsen, Coevolution to the edge of chaos: Coupled fitness landscapes, poised states, and coevolutionary avalanches. *J. Theor. Biol.* **149**, 467–505 (1991).
62. VV Ramasesh, E Dyer, M Raghu, Anatomy of catastrophic forgetting: Hidden representations and task semantics (2020).
63. HE Stanley, VK Wong, Introduction to phase transitions and critical phenomena. *Am. J. Phys.* **40**, 927–928 (1972).
64. N Bertschinger, T Natschläger, Real-time computation at the edge of chaos in recurrent neural networks. *Neural Comput.* **16**, 1413–1436 (2004).
65. P Rämö, S Kauffman, J Kesseli, O Yli-Harja, Measures for information propagation in boolean networks. *Phys. D: Nonlinear Phenom.* **227**, 100–104 (2007).
66. S Kauffman, C Peterson, B Samuelsson, C Troein, Genetic networks with canalizing boolean rules are always stable. *Proc. Natl. Acad. Sci.* **101**, 17102–17107 (2004).
67. WL Shew, H Yang, S Yu, R Roy, D Plenz, Information capacity and transmission are maximized in balanced cortical networks with neuronal avalanches. *J. Neurosci.* **31**, 55–63 (2011).
68. T Mora, W Bialek, Are biological systems poised at criticality? *J. Stat. Phys.* **144**, 268–302 (2011).
69. D Plenz, TC Thiagarajan, The organizing principles of neuronal avalanches: cell assemblies in the cortex? *Trends Neurosci.* **30**, 101–110 (2007).
70. Ł Kuśmierz, S Ogawa, T Toyozumi, Edge of chaos and avalanches in neural networks with heavy-tailed synaptic weight distribution. *Phys. Rev. Lett.* **125** (2020).
71. K Kandera, T Lorimer, R Stoop, Avalanche and edge-of-chaos criticality do not necessarily co-occur in neural networks. *Chaos: An Interdiscip. J. Nonlinear Sci.* **27**, 047408 (2017).
72. IC Fiebelkorn, S Kastner, A rhythmic theory of attention. *Trends Cogn. Sci.* **23**, 87–101 (2019).
73. IC Fiebelkorn, YB Saalman, S Kastner, Rhythmic sampling within and between objects despite sustained attention at a cued location. *Curr. Biol.* **23**, 2553–2558 (2013).
74. M Kirchhoff, T Parr, E Palacios, K Friston, J Kiverstein, The markov blankets of life: autonomy, active inference and the free energy principle. *J. The Royal Soc. Interface* **15**, 20170792 (2018).
75. M Lungarella, O Sporns, Information self-structuring: key principle for learning and development in *Proc. of the 4th Int. Conf. on Development and Learning*. (IEEE), pp. 25–30 (2005).
76. K Friston, C Thornton, A Clark, Free-energy minimization and the dark-room problem. *Front. Psychol.* **3** (2012).
77. J Bruineberg, E Rietveld, Self-organization, free energy minimization, and optimal grip on a field of affordances. *Front. Hum. Neurosci.* **8** (2014).
78. RK Logan, What is information?: Why is it relativistic and what is its relationship to materiality, meaning and organization. *Information* **3**, 68–91 (2012).
79. DJ Nicholson, Is the cell really a machine? *J. Theor. Biol.* **477**, 108–126 (2019).
80. R Pfeifer, M Lungarella, F Iida, Self-organization, embodiment, and biologically inspired robotics. *Science* **318**, 1088–1093 (2007).
81. M Merleau-Ponty, *The structure of behavior*. (Duchesne University Press), (1983).
82. J Bongard, R Pfeifer, *How the Body Shapes the Way We Think*. (MIT Press, Cambridge, Massachusetts), (2006).
83. G Buzsáki, Neuronal oscillations in cortical networks. *Science* **304**, 1926–1929 (2004).
84. D Zenklusen, DR Larson, RH Singer, Single-RNA counting reveals alternative modes of gene expression in yeast. *Nat. Struct. & Mol. Biol.* **15**, 1263–1271 (2008).
85. SP MacEvoy, TD Hanks, MA Paradiso, Macaque v1 activity during natural vision: Effects of natural scenes and saccades. *J. Neurophysiol.* **99**, 460–472 (2008).
86. C Rajkai, et al., Transient cortical excitation at the onset of visual fixation. *Cereb. Cortex* **18**, 200–209 (2007).
87. ZF Mainen, TJ Sejnowski, Influence of dendritic structure on firing pattern in model neocortical neurons. *Nature* **382**, 363–366 (1996).
88. A Paré, et al., Visualization of individual scr mRNAs during drosophila embryogenesis yields evidence for transcriptional bursting. *Curr. Biol.* **19**, 2037–2042 (2009).
89. A Raj, CS Peskin, D Tranchina, DY Vargas, S Tyagi, Stochastic mRNA synthesis in mammalian cells. *PLoS Biol.* **4**, e309 (2006).
90. L Cai, N Friedman, XS Xie, Stochastic protein expression in individual cells at the single molecule level. *Nature* **440**, 358–362 (2006).
91. RD Kamm, et al., Perspective: The promise of multi-cellular engineered living systems. *APL Bioeng.* **2**, 040901 (2018).
92. S Kriegman, D Blackiston, M Levin, J Bongard, A scalable pipeline for designing reconfigurable organisms. *Proc. Natl. Acad. Sci.* **117**, 1853–1859 (2020).
93. H Lipson, JB Pollack, Automatic design and manufacture of robotic lifeforms. *Nature* **406**, 974–978 (2000).
94. CT Mueller, JA Ochsendorf, Combining structural performance and designer preferences in evolutionary design space exploration. *Autom. Constr.* **52**, 70–82 (2015).
95. S Kriegman, Ph.D. thesis (University of Vermont) (2020).

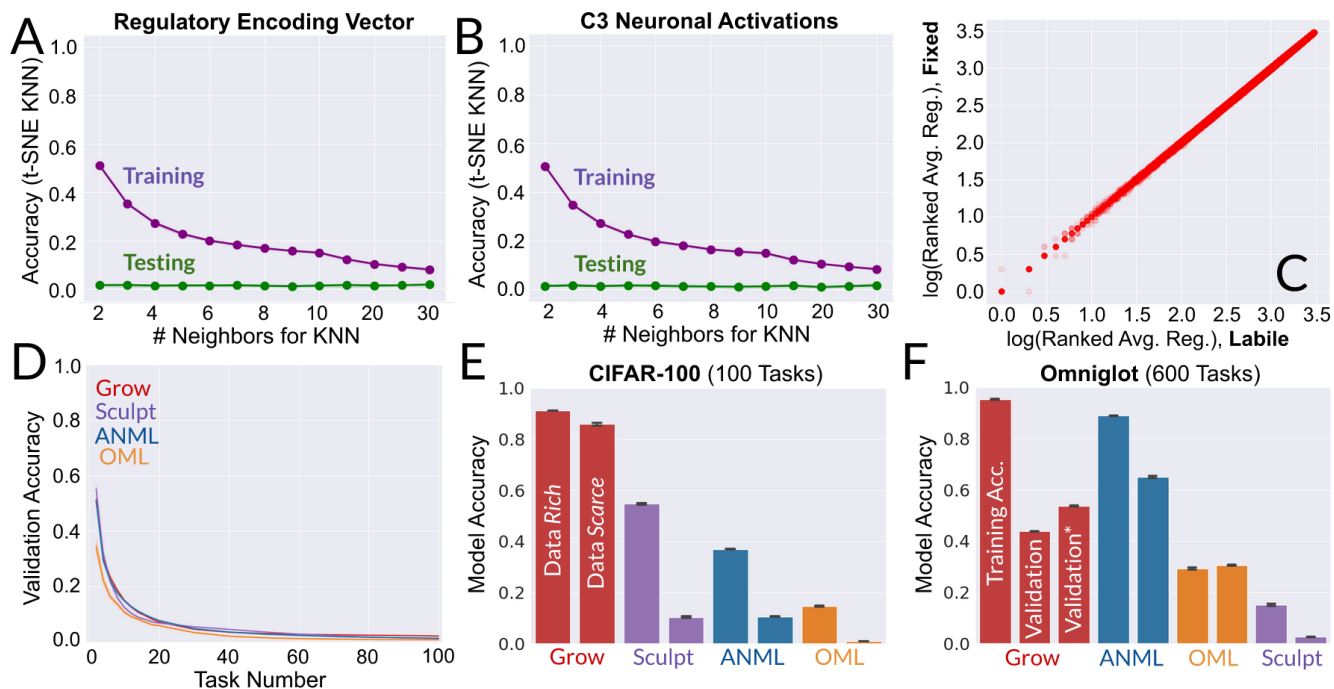


**Fig. 5.** (A) Dimensionally reduced regulatory encoding vectors are not identifiable by class. Following dimensionality reduction to two dimensions through a combination of PCA (50 components) and t-SNE, K-Nearest Neighbors for class prediction was performed. These results show that images belonging to a particular class are not represented by the regulator more similarly than images belonging to other classes. If they were, class prediction by clustering would be high. Confidence intervals report standard deviation across all runs ( $n=25$ ). (B) Representations in the classifier are not clustered by class either. Results that are virtually identical to (A) obtain for KNN clustering of representations produced by the third convolutional layer of the classifier. Thus, images that belong to a given class are not represented more similarly by the classifier than images belonging to other classes. Confidence intervals report standard deviation across all runs ( $n=25$ ). (C) The mean regulation that a given image elicits is virtually identical when the regulatory output layers to C3 are made changeable compared to when they are fixed under domain transfer ( $n=25$ ). Thus, images can be roughly classified as either "intrinsically" enhancing or diminishing. (D) Validation accuracy under domain transfer to ImageNet is low for all models. Given the capacity to generalize to unseen images from the same domain used for meta-learning (F), this does not signify an inability to generalize; rather, it reflects the difficulty of generalizing under domain transfer from few images learned sequentially. (E) Training accuracy under domain transfer to CIFAR-100. **Rich:** Grow=91.1%  $\pm$  0.56% (SD), Sculpt=54.7%  $\pm$  2.4%, ANML=37%  $\pm$  1.70%, OML=14.6%  $\pm$  2.6%. **Scarce:** Grow=85.9%  $\pm$  5.12%, Sculpt=10.4%  $\pm$  2.9%, ANML=10.57%  $\pm$  0.73%, OML=1%  $\pm$  0.10%. Accuracy for 600 previously unseen tasks learned sequentially from Omniglot. **Training:** Grow=95.2%  $\pm$  1.4%, Sculpt=15.1%  $\pm$  2.23%, ANML=88.9%  $\pm$  0.59%, OML=29.3%  $\pm$  2.23%. **Validation:** Grow=43.8.2%  $\pm$  0.93%, Sculpt=2.6%  $\pm$  0.28%, ANML=65.06%  $\pm$  2.88%, OML=30.6%  $\pm$  1.04%. When the regulatory output layers that flow to C1, C2, and C3 in Grow are fixed, but the weights they govern are changeable, validation accuracy ("Grow", 3rd bar) increases to 53.75%  $\pm$  1.45%, indicating that inferiority to ANML is partly the result of forgetting over time, which ANML is insulated from by having just a single layer undergo change on this problem.



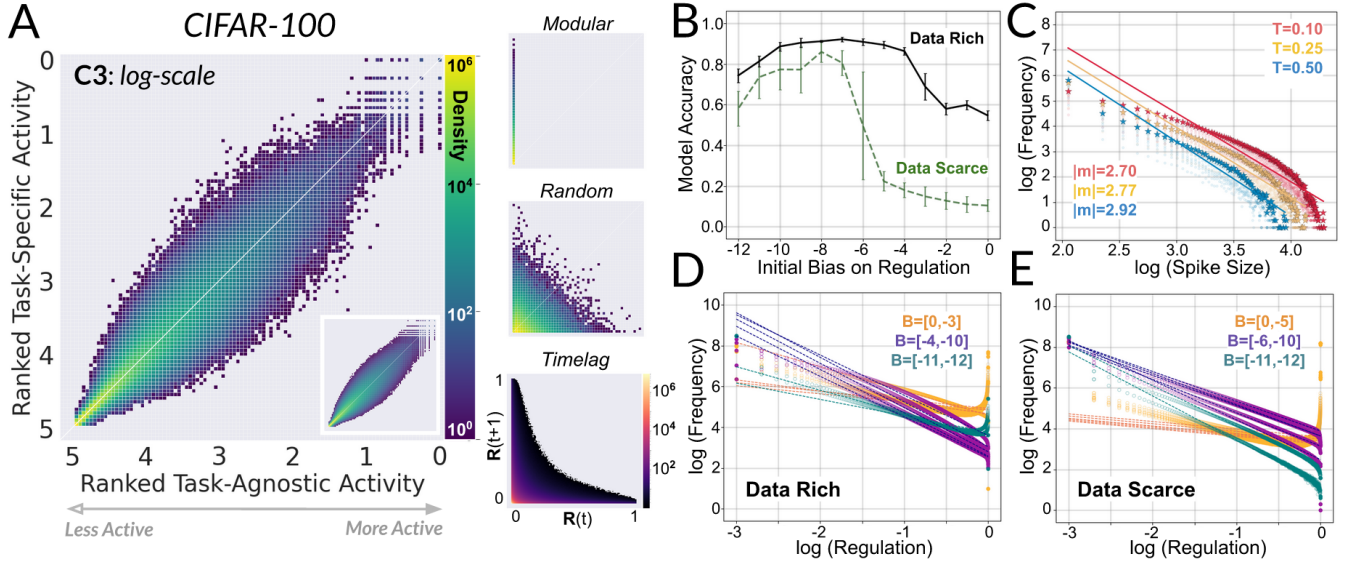


**Fig. 6.** (A) Regulation under domain transfer to CIFAR-100 does not elicit task-specific modularity. Instead, the most active weights on a given task are the most active weights over all tasks, and no synapse drastically changes rank for any individual task (*synaptic recycling*). For each task, regulatory signals are ranked according to their Task-Specific activity (Eq.1) and Task-Agnostic activity (Eq.2). Ranked lists are then transformed to a logarithmic scale (5=least active, 0=most active) and used to fill a two dimensional histogram with 100 bins per dimension (1000 cells in total). The final matrix is filled with data from all 100 tasks and colored by density on a logarithmic scale (60). The inset reports the average over all runs, with cells of density=1 in less than 25% of runs removed, while the main figure reports a single run. See *SI Appendix, Fig.14* for all individual runs, and *Fig.20* for data scarce runs. *Modularity*: as a conceptual aid, we provide a synthetic version of (A) for “perfect” task-specific modularity and Gaussian random regulation. For regulation that is perfectly *Modular*, weights are randomly sorted into 100 disjoint subsets and assigned (i) a random and constant regulatory signal for the task their subset ID corresponds to, and (ii) a value of 0 for every other task, thus producing task-specific modules. For regulation that is *Random*, weights are assigned a Gaussian random regulatory signal for all inputs. *Timelag* (non-synthetic): we observe that highly permissive regulation at time  $t$  is predictive of suppressant regulation at time  $t + 1$ . Thus, synaptic recruitment is highly transient (*synaptic bursting*). Time-lagged regulatory outputs under domain transfer are plotted over all runs by stacking two-dimensional histograms for the 75<sup>th</sup>-99<sup>th</sup> percentile ranked by task-agnostic mean. Centiles ranked lower than 75<sup>th</sup> percentile exhibit even higher transience, if not complete quiescence. We plot the average over the stack of all runs. Outlier cells that have a density less than or equal to 1 post-stacking are masked. Results for individual runs without masking or stacking are presented in *Fig.7A, Fig.8A, Fig.9A, Fig.10A*. (B) Final performance under domain transfer for different initial meta-learning biases on regulation. For each initial bias not equal to 0 (Sculpt) or -8 (Grow), 10 independent models were procured and evaluated for 40 separate runs. (C) Regulation is calibrated to control the *amount* of sensory processing in the classifier, rather than the task-modular *location* where such processing occurs. Increasingly large spikes, which induce more sensory processing, are correspondingly rare, resulting in an approximate power law distribution. This relationship is observed for all convolutional layers (*Fig.Fig.7, Fig.8, Fig.9*). Each color corresponds to a different threshold for which a synapse is said to burst if it receives regulation above that threshold. Distributions over all runs are plotted with a star, while individual runs are plotted as translucent circles. (D,E) High performance under domain transfer to CIFAR-100 (*Fig.3B*) is coincident with particular patterns of regulation, in which highly suppressant regulation dominates and increasingly permissive regulation is correspondingly rare. These patterns only emerge for a certain range of initial meta-learning biases on regulatory output. We believe this reflects a purposive balance of permission and suppression that is analogous to the balance of order and disorder in edge of chaos criticality (61). For data rich (D) and data scarce (E) meta-learning, good regulators (*purple*) exhibit an approximate power law distribution under domain transfer within a specific range of scaling factors. Comparatively worse regulators (*orange* and *teal*) fall outside of this range (more suppressant) or exhibit super-linear distributions (more permissive). We present the highest performing runs for each model. All runs for all models are shown in *Fig.23-29*. Initial biases equal to -9 and -10 for data rich meta-learning fall in the purple cohort of good regulators, but are omitted from (D) for clarity (see *Fig.24*).

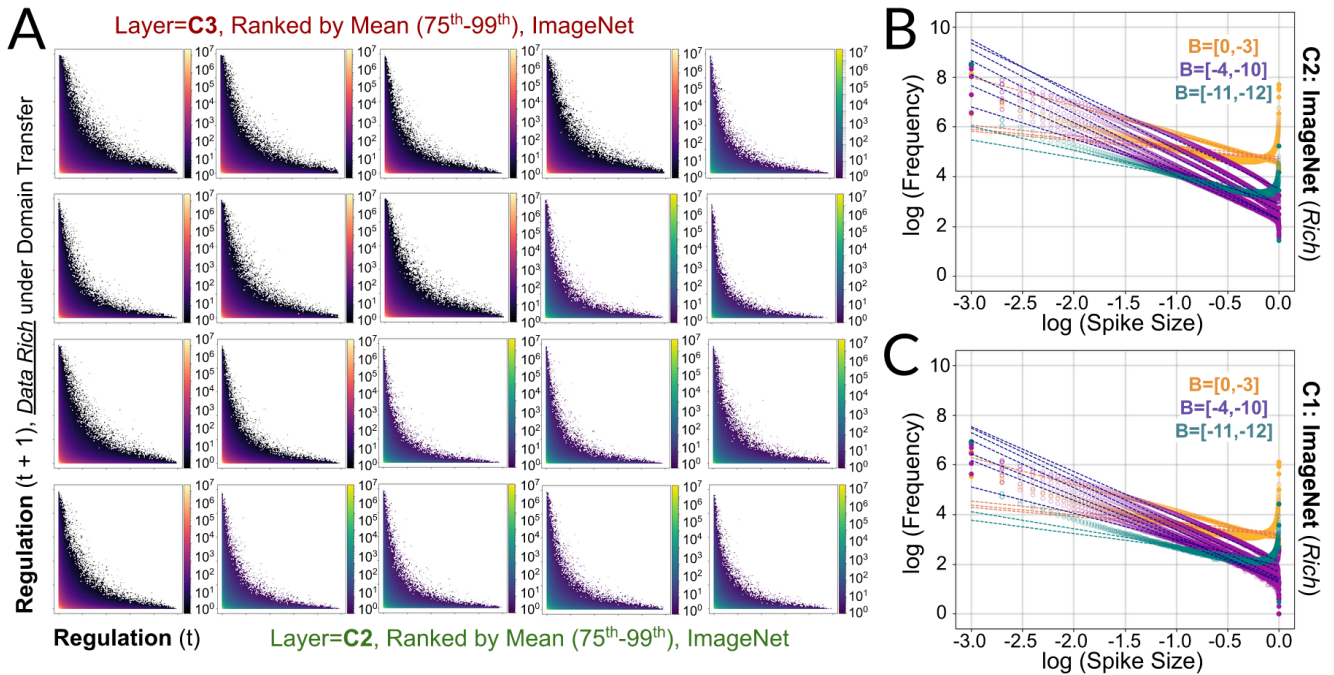


**Fig. 7. (A)** We find that regulation in the data rich condition under domain transfer to ImageNet induces sparse synaptic bursting, which is characterized by highly transient activity in a subset of weights from one time step to the next. Plots are generated using a 2D histogram having 250 bins uniformly spaced between 0 and 1. cells are then colored on a logarithmic scale by density. Results for C3 and C2 are presented for synapses receiving regulation that ranks in the 75th to 99th percentile by task-agnostic mean. We find minor differences between layers in their degree of transience. **(B)** Performant regulation under domain transfer to ImageNet occurs within a particular range of initial meta-learning biases on regulation. Log-log plots for regulation under domain transfer to ImageNet for models with different initial meta-learning biases on regulation. This figure is identical to the one presented in Figure 3D of the main text, but report results for layer C2 in the data rich condition. **(C)** Performant regulation under domain transfer to ImageNet occurs within a particular range of initial meta-learning biases on regulation. This figure is identical to the one presented in Figure 3D of the main text, but report results for layer C1 in the data rich condition.

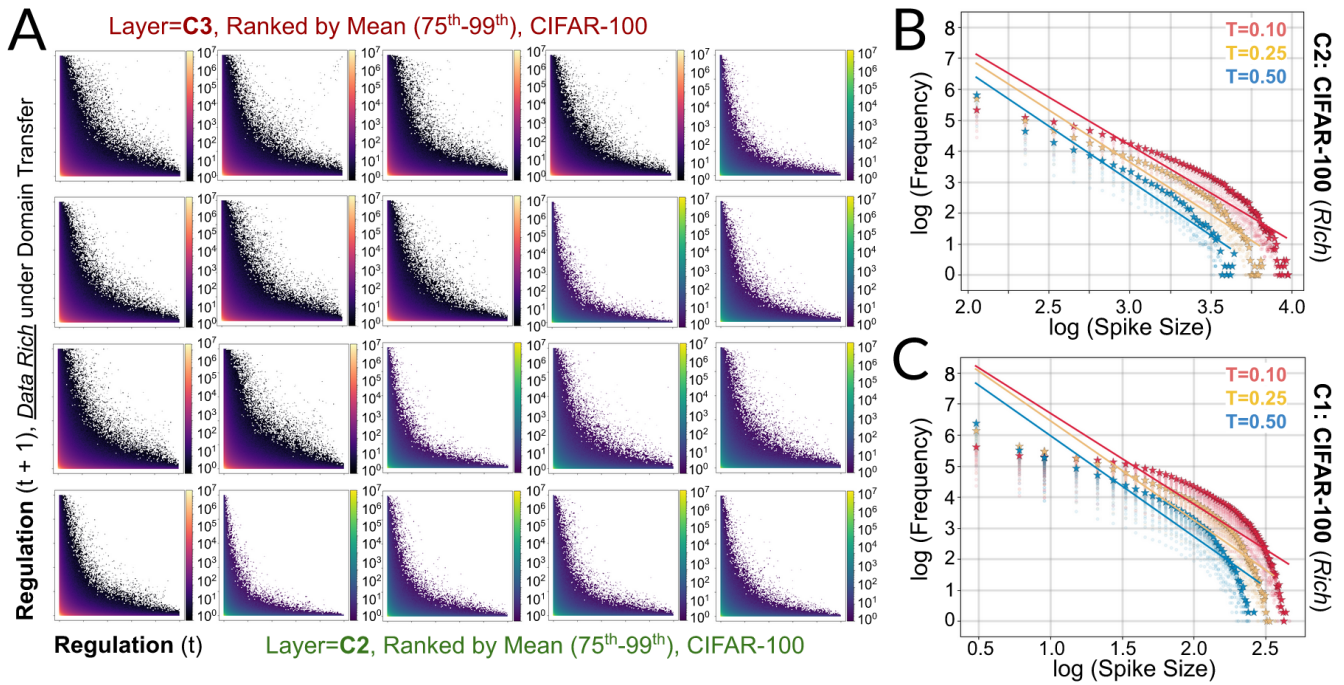


**Fig. 8.** We find that regulation in the data rich condition under domain transfer to CIFAR-100 induces sparse synaptic bursting, which is characterized by highly transient activity in a subset of weights from one time step to the next. Plots are generated using a 2D histogram having 250 bins uniformly spaced between 0 and 1. cells are then colored on a logarithmic scale by density. Results for C3 and C2 are presented for synapses receiving regulation that ranks in the 75th to 99th percentile by task-agnostic mean. We find minor differences between layers in their degree of transience. **(B)** The number of synapses that collectively burst in data rich C2 under domain transfer to CIFAR-100 is approximately power law distributed. Each color corresponds to a different threshold for which a synapse is said to burst if it is above that threshold. Distributions over all runs are plotted with a star, while individual runs are plotted as translucent circles. **(C)** The number of synapses that collectively burst in data rich C1 under domain transfer to CIFAR-100 is approximately power law distributed. Each color corresponds to a different threshold for which a synapse is said to burst if it is above that threshold. Distributions over all runs are plotted with a star, while individual runs are plotted as translucent circles.



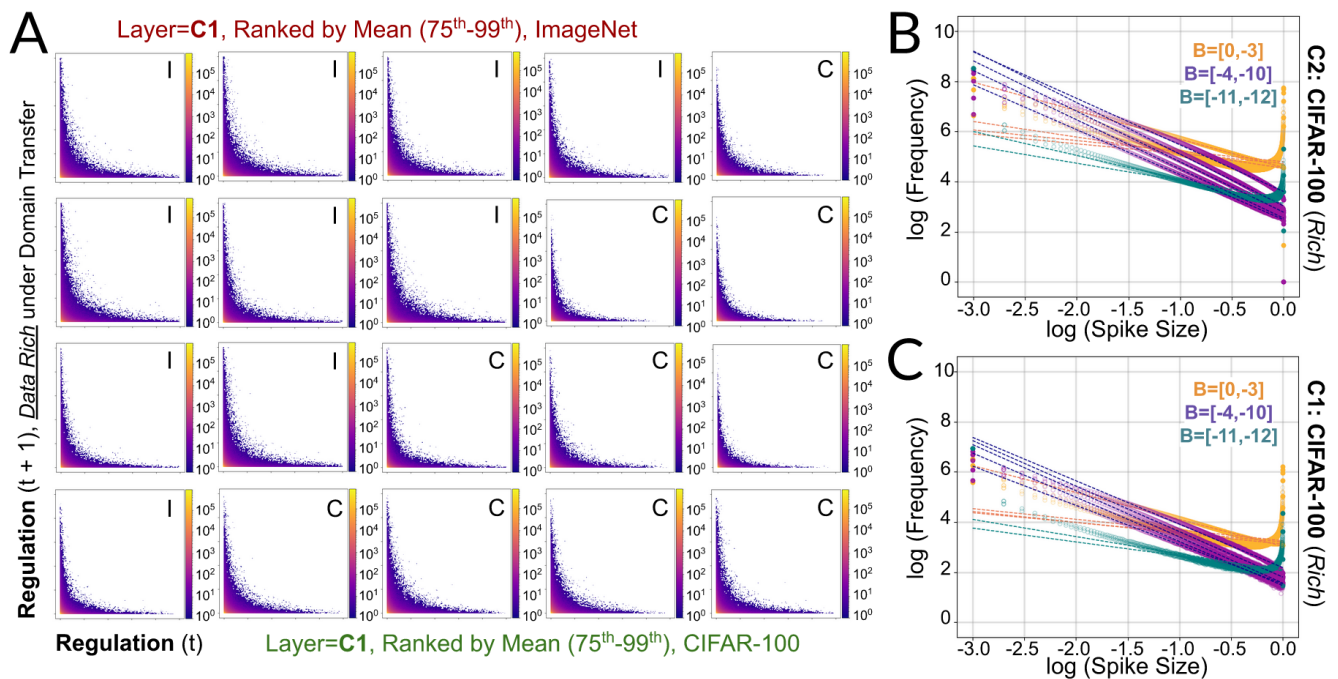


**Fig. 9.** We find that regulation in the data rich condition under domain transfer to ImageNet and CIFAR-100 induces sparse synaptic bursting, which is characterized by highly transient activity in a subset of weights from one time step to the next. Plots are generated using a 2D histogram having 250 bins uniformly spaced between 0 and 1. cells are then colored on a logarithmic scale by density. Results for C1 are presented for synapses receiving regulation that ranks in the 75th to 99th percentile by task-agnostic mean. We find negligible differences in the behavior of C1 between datasets. Results from ImageNet and CIFAR-100 are denoted by the letter in the upper right corner of each subplot. **(B)** Performant regulation under domain transfer to CIFAR-100 occurs within a particular range of initial meta-learning biases on regulation. Log-log plots for regulation under domain transfer to CIFAR-100 for models with different initial meta-learning biases on regulation. This figure is identical to the one presented in Fig.6D, but reports results for layer C2 in the data rich condition. **(C)** Performant regulation under domain transfer to CIFAR-100 occurs within a particular range of initial meta-learning biases on regulation. Log-log plots for regulation under domain transfer to CIFAR-100 for models with different initial meta-learning biases on regulation. This figure is identical to the one presented in Fig.6D, but reports results for layer C1 in the data rich condition.

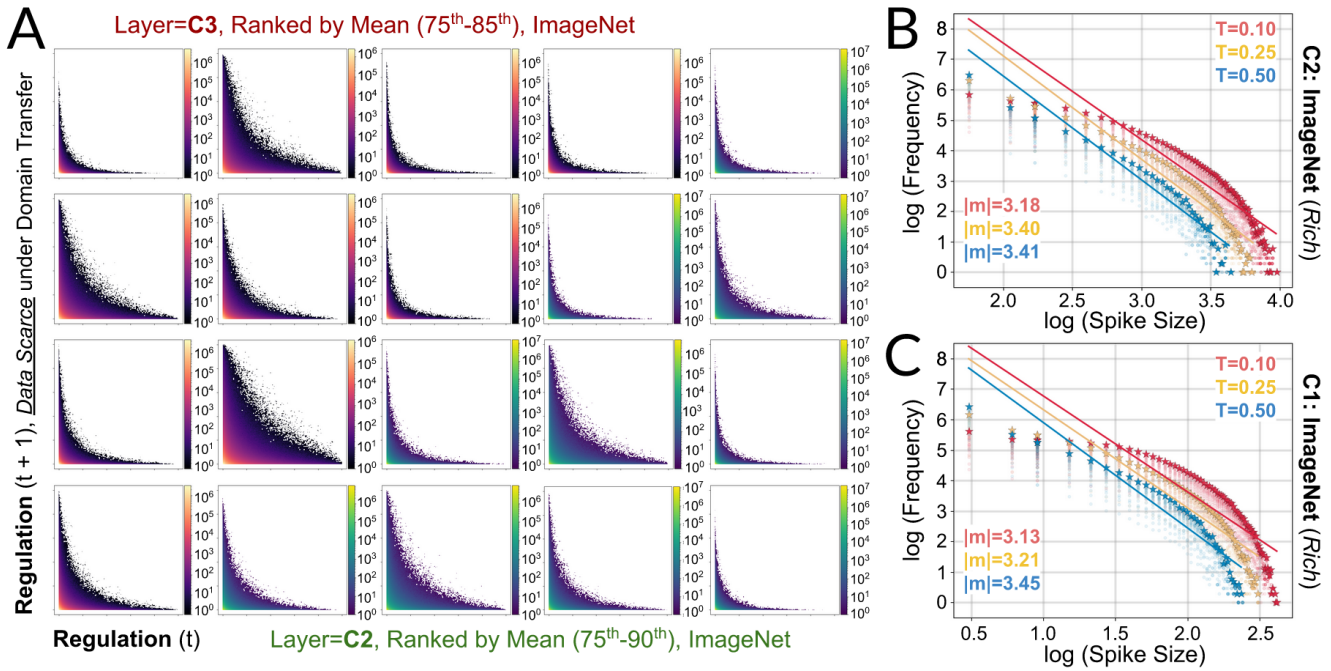


**Fig. 10.** We find that regulation in the data scarce condition under domain transfer to ImageNet induces sparse synaptic bursting, which is characterized by highly transient activity in a subset of weights from one time step to the next. Plots are generated using a 2D histogram having 250 bins uniformly spaced between 0 and 1. Cells are then colored on a logarithmic scale by density. Results for C3 and C2 are presented for synapses receiving regulation that ranks by task-agnostic mean in the 75th-85th percentile and 75th-90th percentile, respectively. **(B)** The number of synapses that collectively burst in data rich C2 under domain transfer to ImageNet is approximately power law distributed. Each color corresponds to a different threshold for which a synapse is said to burst if it is above that threshold. Distributions over all runs are plotted with a star, while individual runs are plotted as translucent circles. **(C)** The number of synapses that collectively burst in data rich C1 under domain transfer to ImageNet is approximately power law distributed. Each color corresponds to a different threshold for which a synapse is said to burst if it is above that threshold. Distributions over all runs are plotted with a star, while individual runs are plotted as translucent circles.

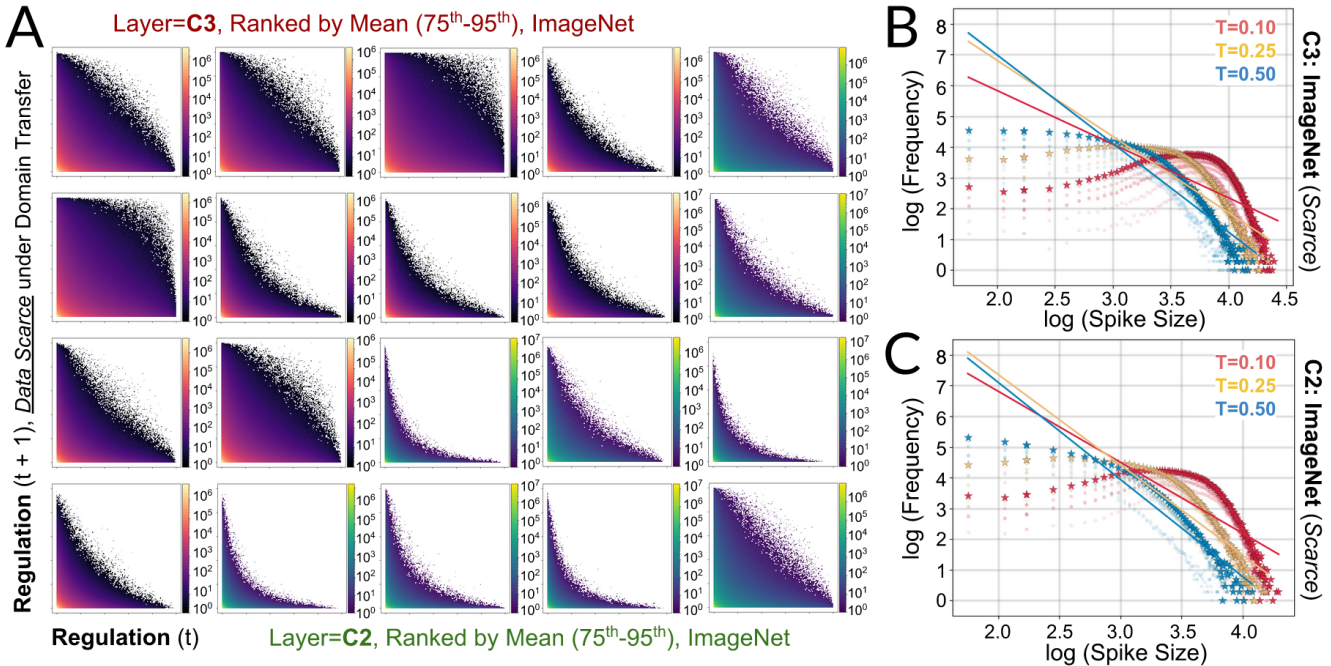


**Fig. 11.** **(A)** Synapses that rank higher in task-agnostic mean for the data scarce condition are less transient under domain transfer to ImageNet than in the data rich condition (Fig. 7). This figure is identical to Fig. 10, but shows the behavior of the top 75-95 centiles ranked by task-agnostic mean. Thus, synaptic bursting in the data scarce condition, as demonstrated in the main text, tends to be less sparse than the data rich condition. **(B)** The distribution of spike sizes in C3 for the data scarce condition under domain transfer to ImageNet is noticeably different than the distribution of spike sizes in C3 for the data rich condition. However, the distribution is still approximately linear in log-log space for larger spike sizes. **(C)** The distribution of spike sizes in C2 for the data scarce condition under domain transfer to ImageNet is noticeably different than the distribution of spike sizes in C2 for the data rich condition. However, the distribution is still approximately linear in log-log space for larger spike sizes.

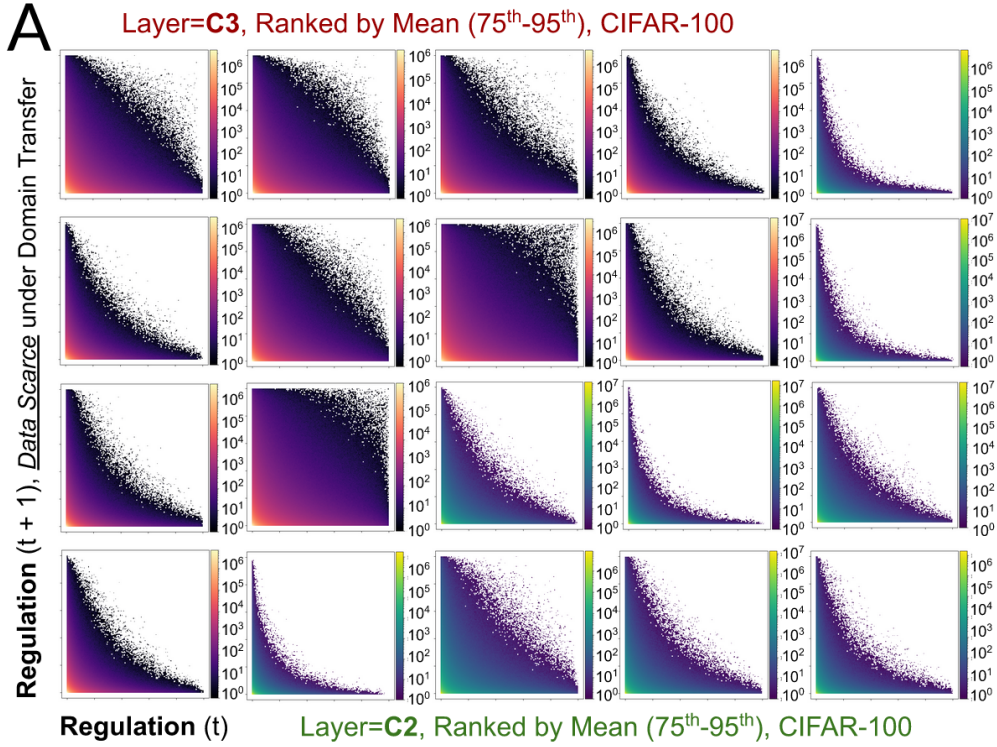


**Fig. 12.** Synapses that rank higher in task-agnostic mean for the data scarce condition are less transient under domain transfer to CIFAR-100 than in the data rich condition (Fig.8). This figure is identical to Fig.10, but shows the behavior of the top 75th-95th centiles ranked by task-agnostic mean under domain transfer to CIFAR-100. Thus, synaptic bursting in the data scarce condition, as demonstrated in the main text, tends to be less sparse than the data rich condition.

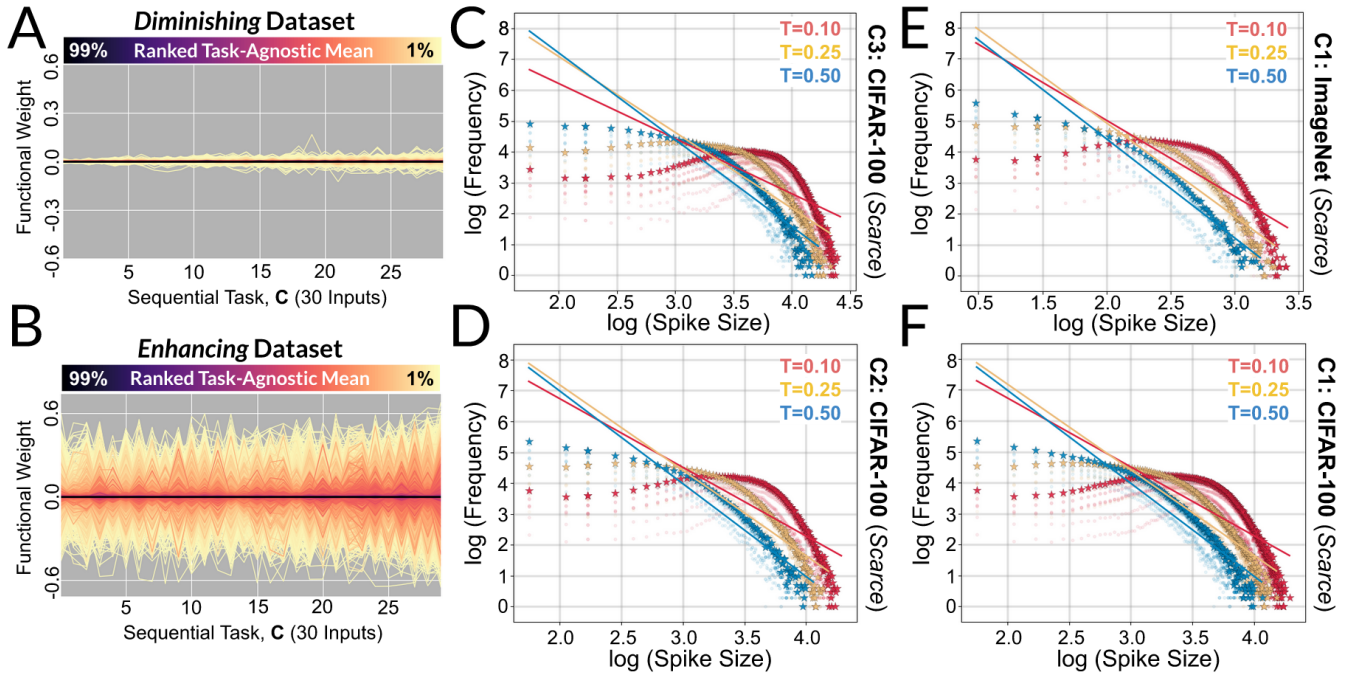


**Fig. 13.** (A) Images from the diminishing dataset result in diminished sensory processing in the classifier. We plot functional weights in C3 over a randomly sampled task window for a randomly sampled run. Functional weights are synaptic values post-regulatory intervention, and are colored by centile according to ranked mean computed over all domain transfer tasks. (B) Images from the enhancing dataset result in enhanced sensory processing in the classifier. We plot functional weights in C3 over a randomly sampled task window for a randomly sampled run. Functional weights are synaptic values post-regulatory intervention, and are colored by centile according to ranked mean computed over all domain transfer tasks. (C) The distribution of spike sizes in C3 for the data scarce condition under domain transfer to CIFAR-100 is noticeably different than the distribution of spike sizes in C3 for the data rich condition. However, the distribution is still approximately linear in log-log space for larger spike sizes. (D) The distribution of spike sizes in C2 for the data scarce condition under domain transfer to CIFAR-100 is noticeably different than the distribution of spike sizes in C2 for the data rich condition. However, the distribution is still approximately linear in log-log space for larger spike sizes. (E) Distribution of spike sizes in C1 for the data scarce condition under domain transfer to ImageNet. (F) Distribution of spike sizes in C1 for the data scarce condition under domain transfer to CIFAR-100.



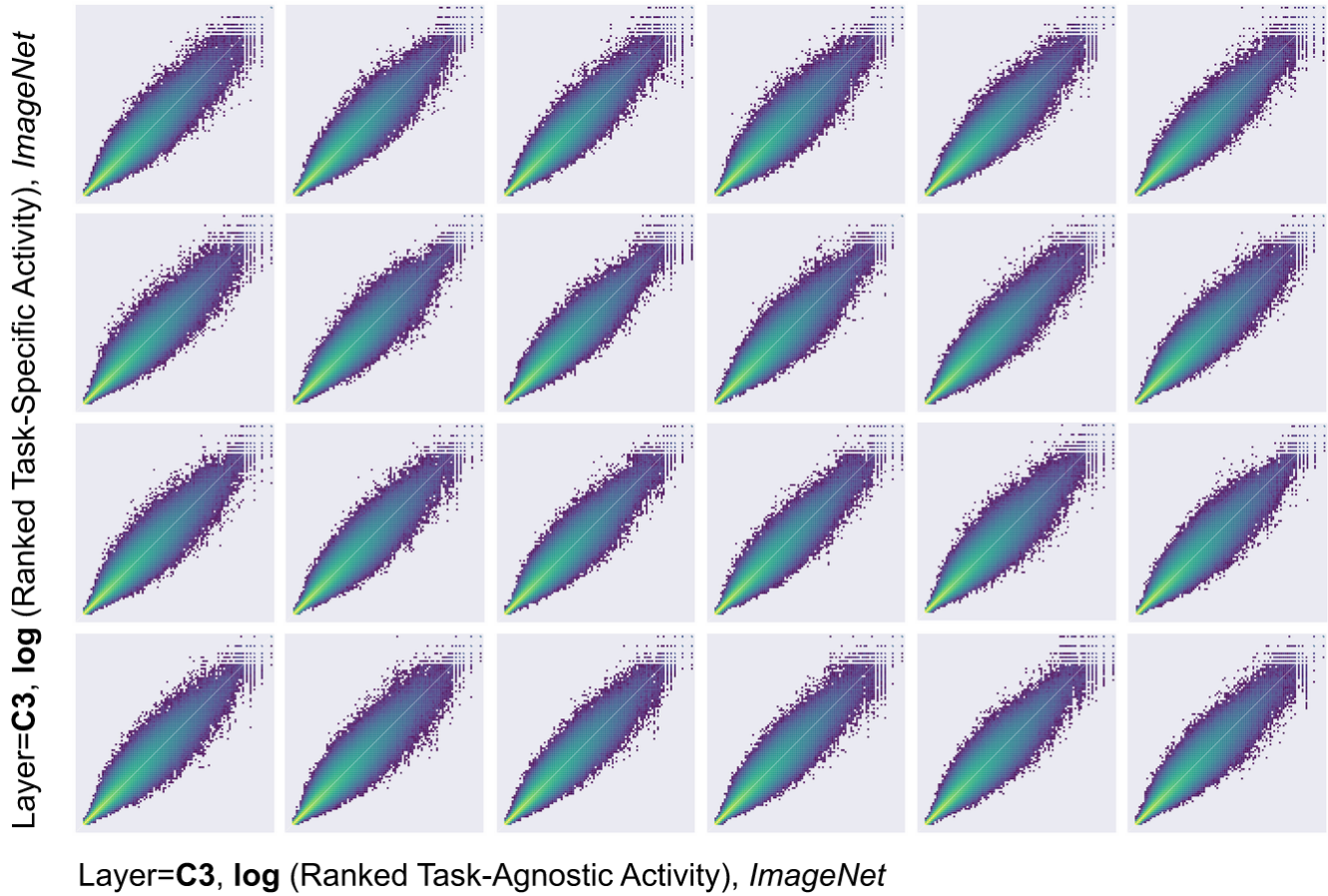


**Fig. 14.** Regulation in C3 of the data rich condition under domain transfer to ImageNet does not elicit task-specific modularity. Instead, the most active weights on a given task are the most active weights over all tasks, and no synapse dramatically changes rank for any individual task. See Fig.6, and Figure 3 in the main text, for details regarding figure construction. Here we present results for a single trial for each of the remaining 24 models.



Layer=C3, log (Ranked Task-Specific Activity), CIFAR-100



Layer=C3, log (Ranked Task-Agnostic Activity), CIFAR-100

**Fig. 15.** Regulation in C3 of the data rich condition under domain transfer to CIFAR-100 does not elicit task-specific modularity. Instead, the most active weights on a given task are the most active weights over all tasks, and no synapse dramatically changes rank for any individual task. See Fig.6, and Figure 3 in the main text, for details regarding figure construction. Here we present results for a single trial for the remaining 24 independent models.

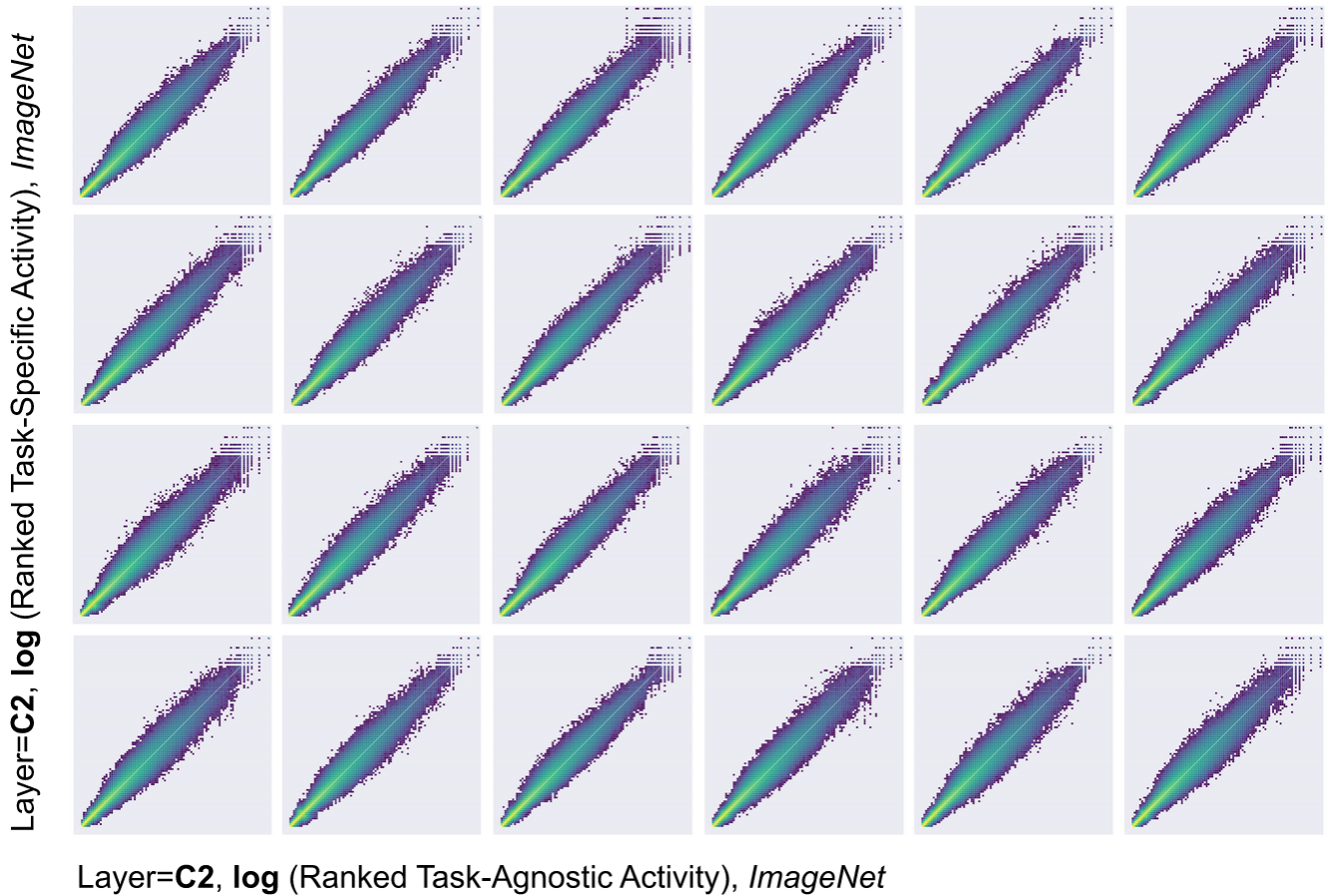
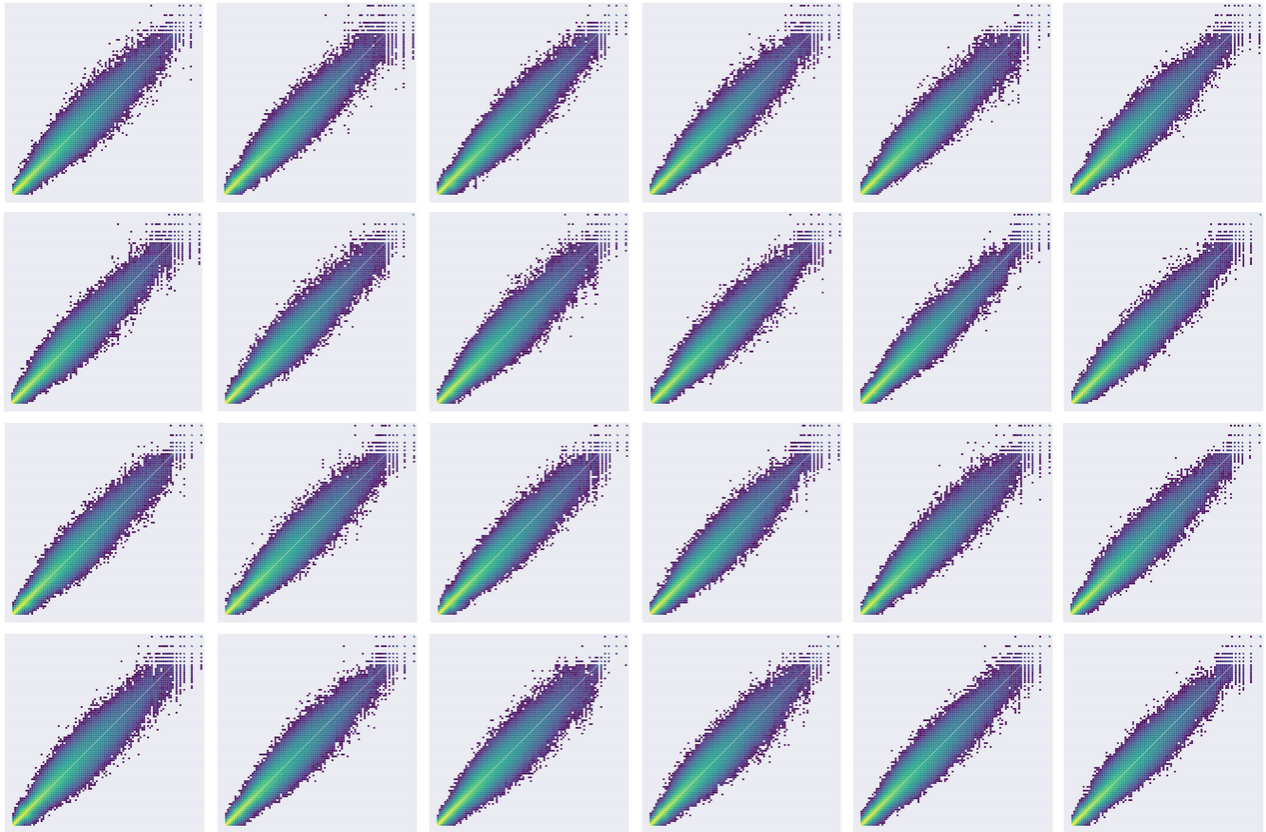


**Fig. 16.** Regulation in C2 of the data rich condition under domain transfer to ImageNet does not elicit task-specific modularity. Instead, the most active weights on a given task are the most active weights over all tasks, and no synapse dramatically changes rank for any individual task. See Fig.6, and Figure 3 in the main text, for details regarding figure construction. Here we present results for a single trial for 24 independent models. Compared to results for regulation of C3 under domain transfer to ImageNet, regulation of C2 is noticeably less context-sensitive. This may be attributed to the common observation that successive layers in neural networks attend to decreasingly generic properties of inputs. Nevertheless, context-dependent modules, which are an extreme form of context sensitivity, are not present in any of the convolutional layers.

Layer=C2, log (Ranked Task-Specific Activity), CIFAR-100



Layer=C2, log (Ranked Task-Agnostic Activity), CIFAR-100

Fig. 17. Regulation in C2 of the data rich condition under domain transfer to CIFAR-100 does not elicit task-specific modularity. Instead, the most active weights on a given task are the most active weights over all tasks, and no synapse dramatically changes rank for any individual task. See Fig.6, and Figure 3 in the main text, for details regarding figure construction. Here we present results for a single trial for each of the remaining 24 models. Compared to results for regulation of C3 under domain transfer to CIFAR-100, regulation of C2 is noticeably less context-sensitive. This may be attributed to the common observation that successive layers in neural networks attend to decreasingly generic properties of inputs. Nevertheless, context-dependent modules, which are an extreme form of context sensitivity, are not present in any of the convolutional layers.

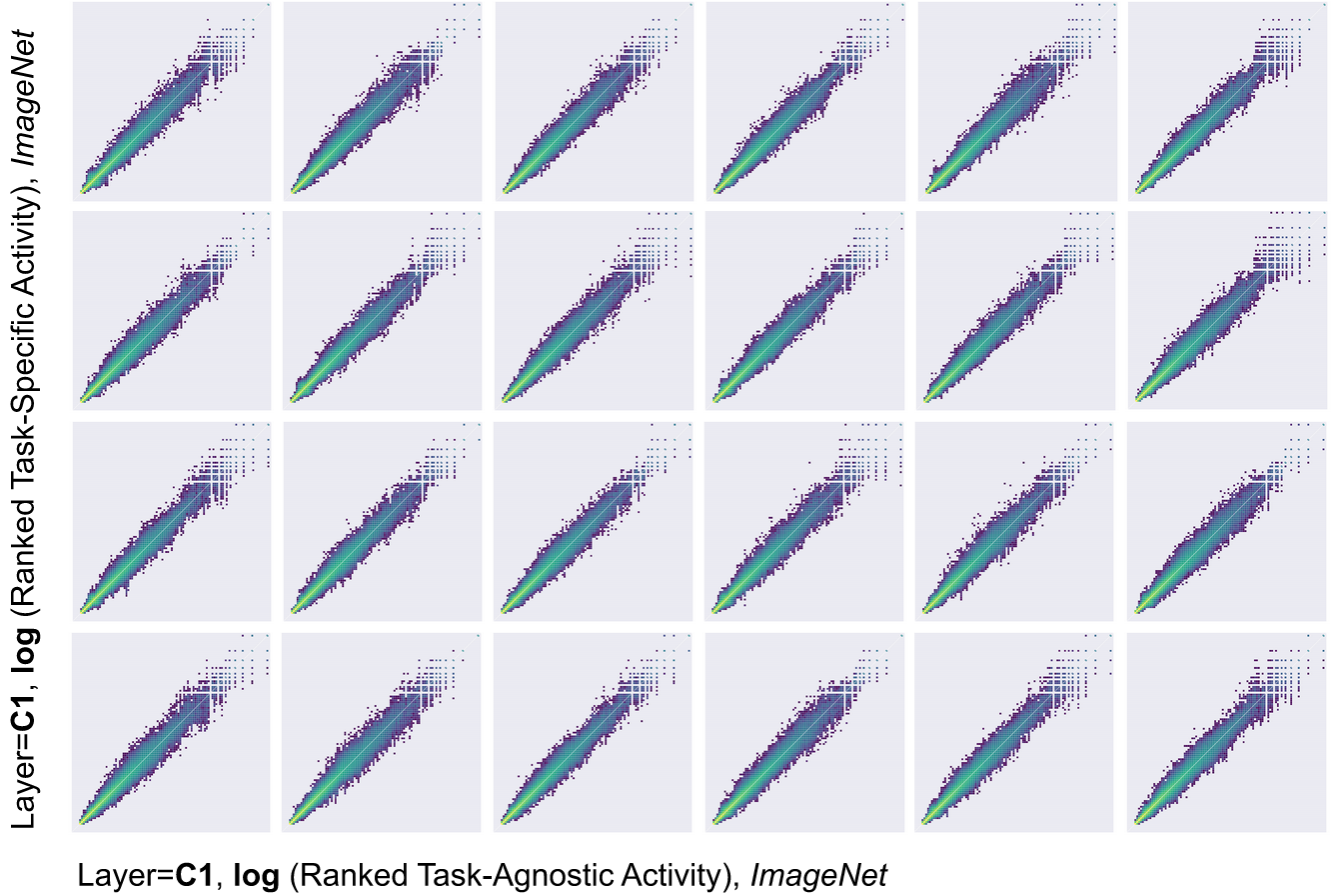


**Fig. 18.** Regulation in C1 of the data rich condition under domain transfer to ImageNet does not elicit task-specific modularity. Instead, the most active weights on a given task are the most active weights over all tasks, and no synapse dramatically changes rank for any individual task. See Fig.6, and Figure 3 in the main text, for details regarding figure construction. Here we present results for a single trial for each of the remaining 24 models. Compared to results for regulation of C3 and C2 under domain transfer to ImageNet, regulation of C1 is noticeably less context-sensitive. This may be attributed to the common observation that successive layers in neural networks attend to decreasingly generic properties of inputs. Nevertheless, context-dependent modules, which are an extreme form of context sensitivity, are not present in any of the convolutional layers.



Layer=C1, log (Ranked Task-Specific Activity), CIFAR-100



Layer=C1, log (Ranked Task-Agnostic Activity), CIFAR-100

**Fig. 19.** Regulation in C1 of the data rich condition under domain transfer to CIFAR-100 does not elicit task-specific modularity. Instead, the most active weights on a given task are the most active weights over all tasks, and no synapse dramatically changes rank for any individual task. See Fig. 6, and Figure 3 in the main text, for details regarding figure construction. Here we present results for a single trial for each of the remaining 24 models. Compared to results for regulation of C3 and C2 under domain transfer to CIFAR-100, regulation of C1 is noticeably less context-sensitive. This may be attributed to the common observation that successive layers in neural networks attend to decreasingly generic properties of inputs. Nevertheless, context-dependent modules, which are an extreme form of context sensitivity, are not present in any of the convolutional layers.

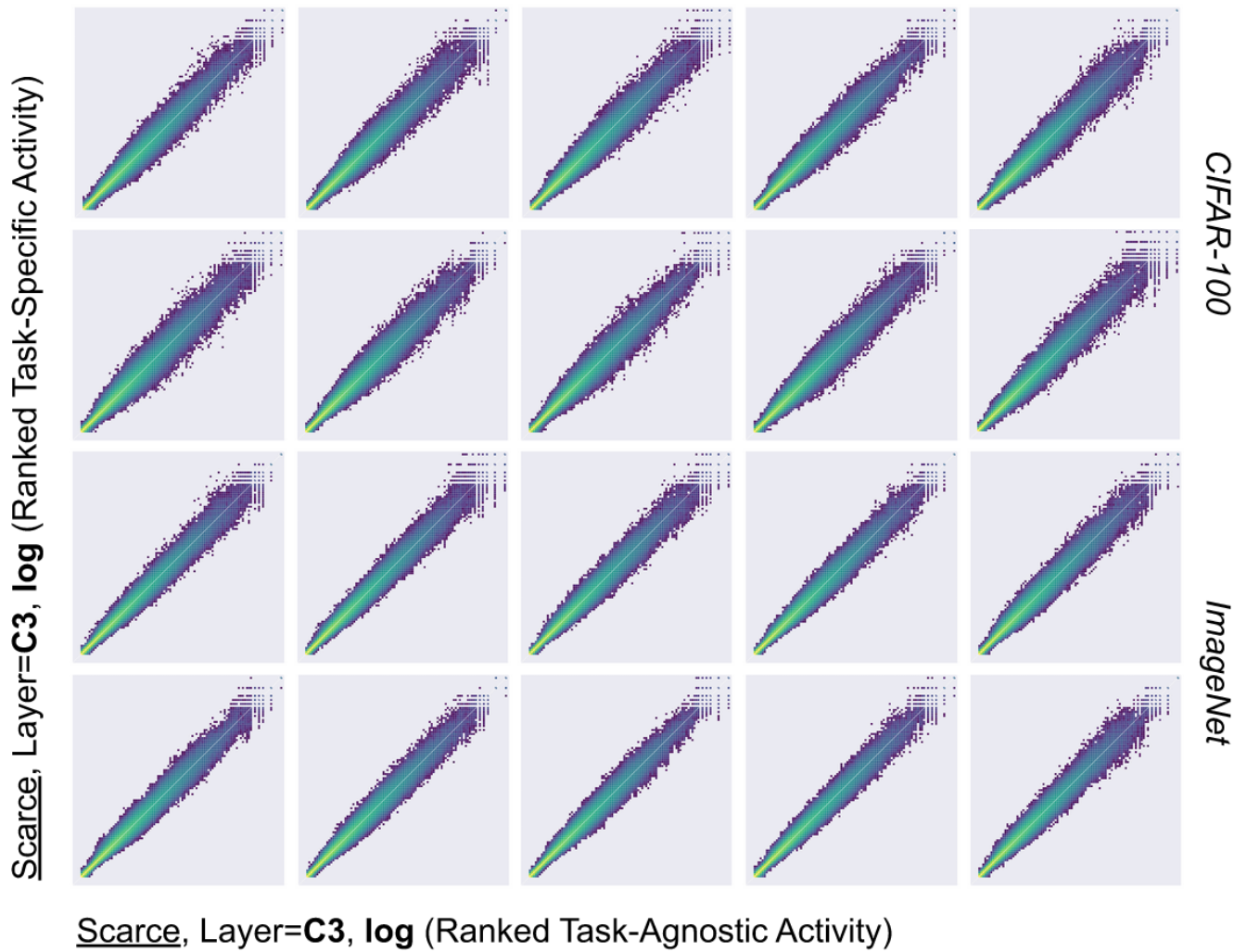


**Fig. 20.** The lack of task-specific modularity observed in the regulation of C3 in the data rich condition is recapitulated for regulation of C3 in the data scarce condition. We also find that regulation in the data scarce condition is noticeably less context sensitive than in the data rich condition. This might be explained by the inability to form strong feature specific regulatory responses from limited meta-learning data. Thus, we find that synaptic recycling in C3 is more strongly pronounced in the data scarce condition.

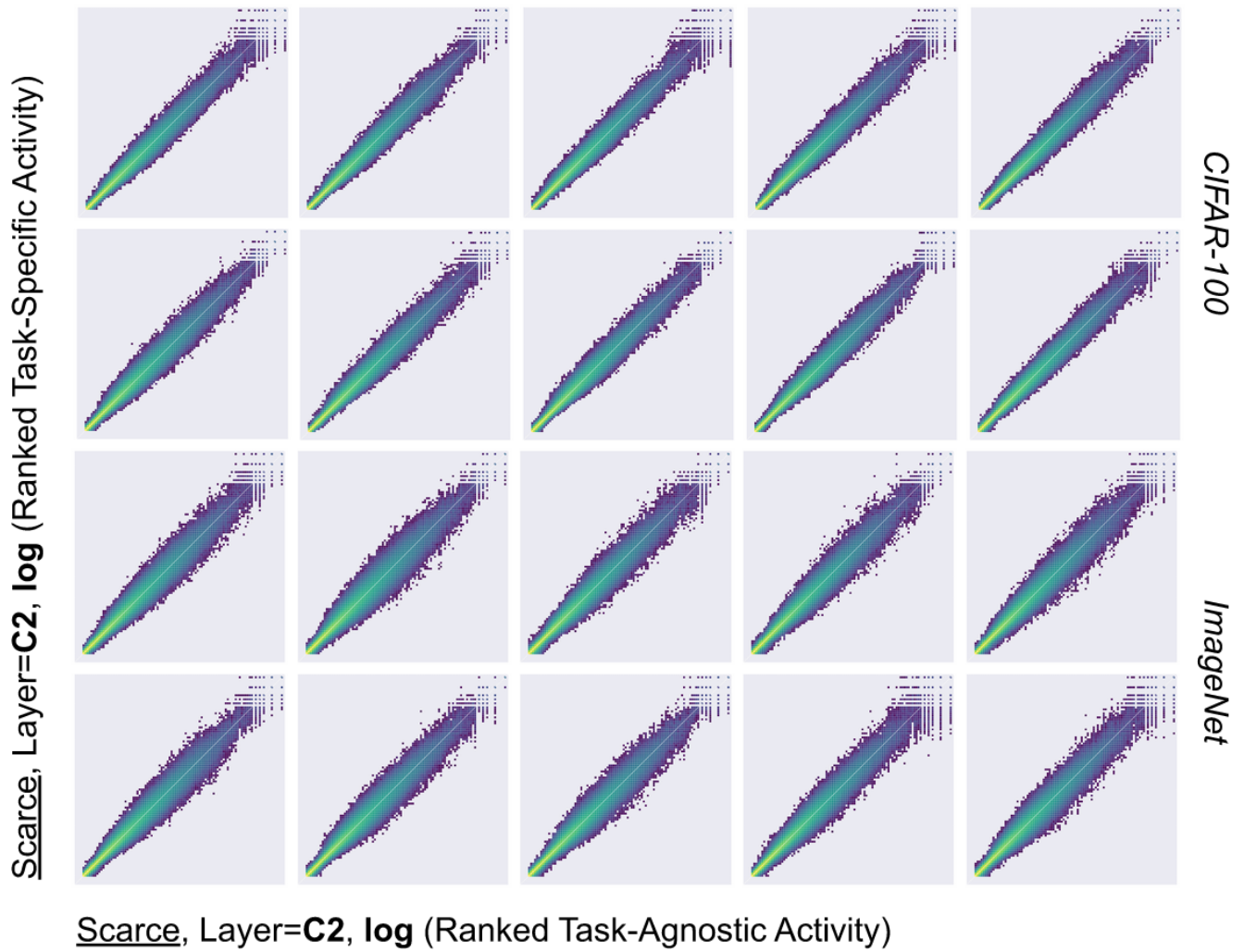


**Fig. 21.** The lack of task-specific modularity observed in the regulation of C2 in the data rich condition is recapitulated for regulation of C2 in the data scarce condition. We also find that regulation in the data scarce condition is noticeably less context sensitive than in the data rich condition. This might be explained by the inability to form strong feature specific regulatory responses from limited meta-learning data. Thus, we find that synaptic recycling in C2 is more strongly pronounced in the data scarce condition.

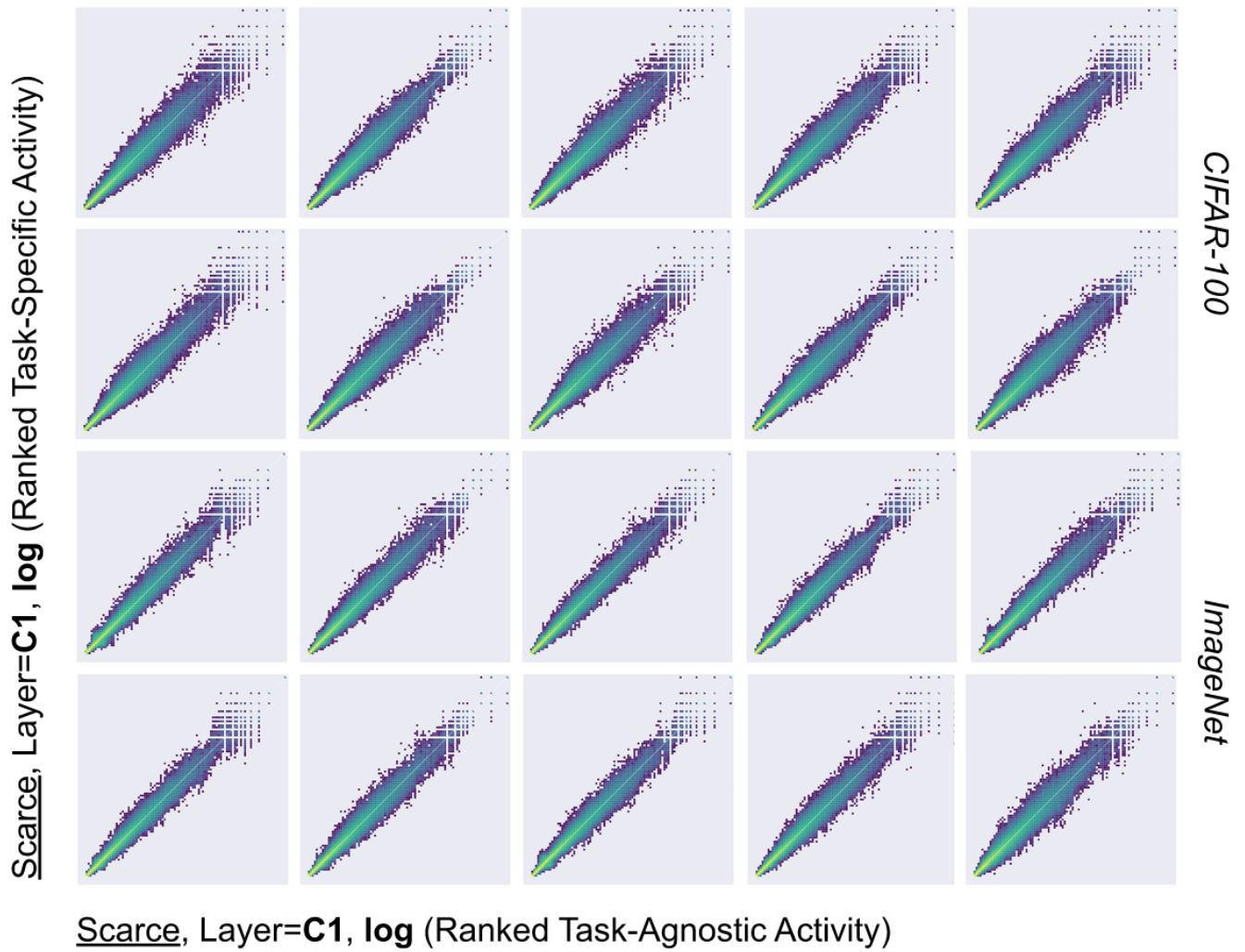


**Fig. 22.** The lack of task-specific modularity observed in the regulation of C1 in the data rich condition is recapitulated for regulation of C1 in the data scarce condition. We also find that regulation in the data scarce condition is noticeably less context sensitive than in the data rich condition. This might be explained by the inability to form strong feature specific regulatory responses from limited meta-learning data. Thus, we find that synaptic recycling in C1 is more strongly pronounced in the data scarce condition.



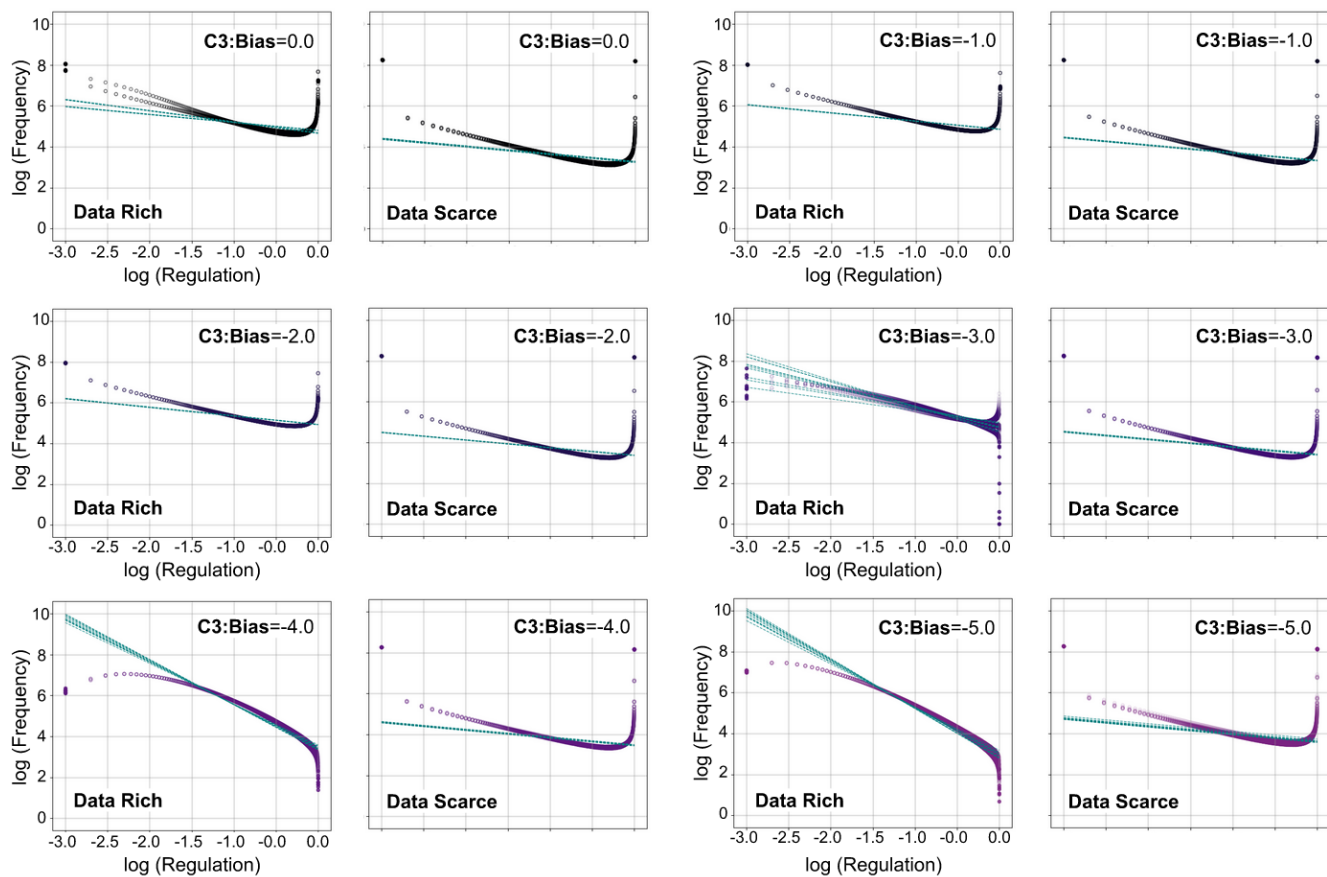


**Fig. 23.** We present individual log-log plots for regulation under domain transfer to ImageNet for each set of 10 runs per initial meta-learning bias setting for both data rich and data scarce meta-learning. These results continue in Fig.24. Qualitatively identical results for domain transfer to CIFAR-100 will be made available for download. But see Fig.29.

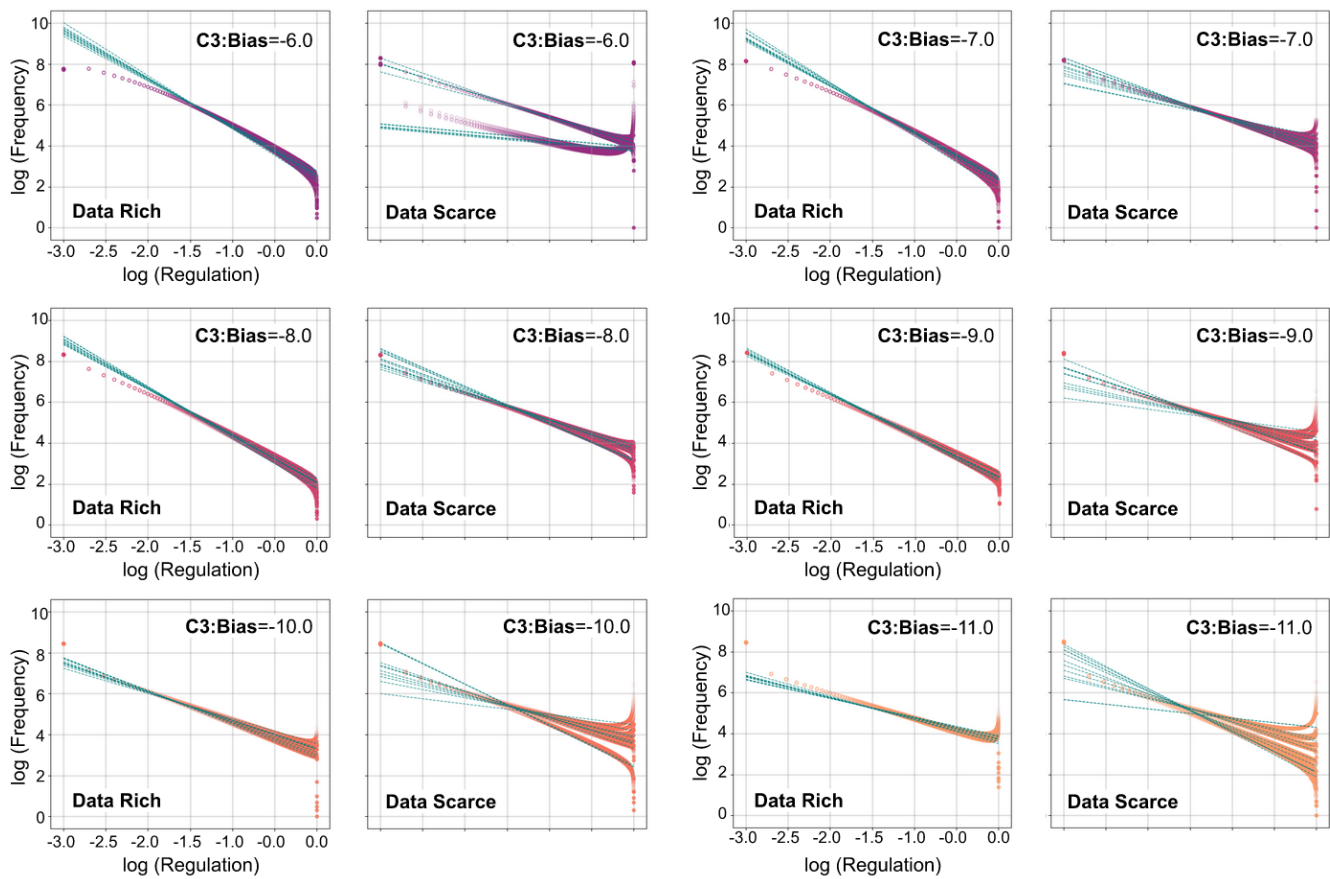


**Fig. 24.** We present individual log-log plots for regulation under domain transfer to ImageNet for each set of 10 runs per initial meta-learning bias setting for both data rich and data scarce meta-learning. These results continue in Fig.25. Qualitatively identical results for domain transfer to CIFAR-100 will be made available for download. But see Fig.29.

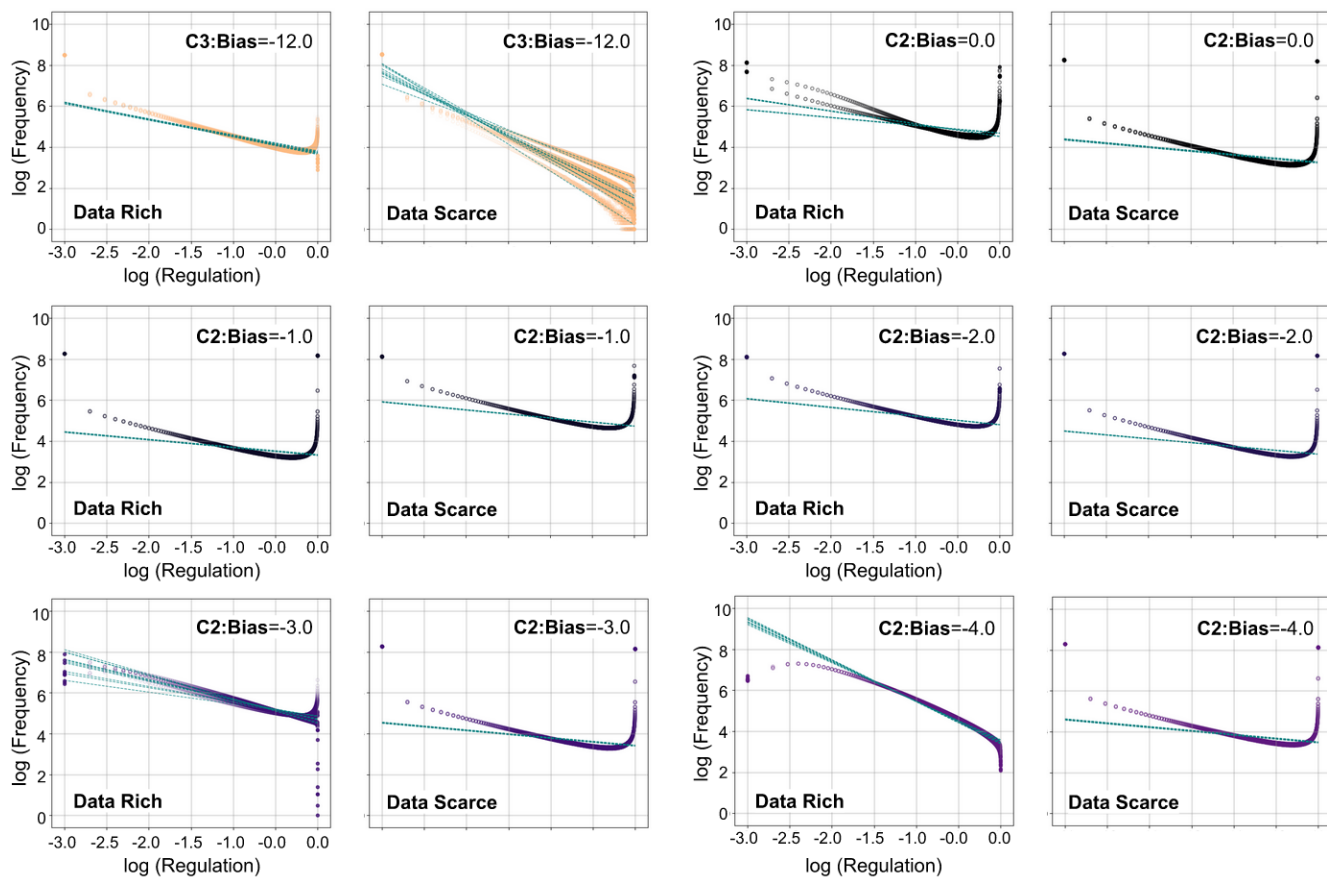


**Fig. 25.** We present individual log-log plots for regulation under domain transfer to ImageNet for each set of 10 runs per initial meta-learning bias setting for both data rich and data scarce meta-learning. These results continue in Fig.26. Qualitatively identical results for domain transfer to CIFAR-100 will be made available for download. But see Fig.29.

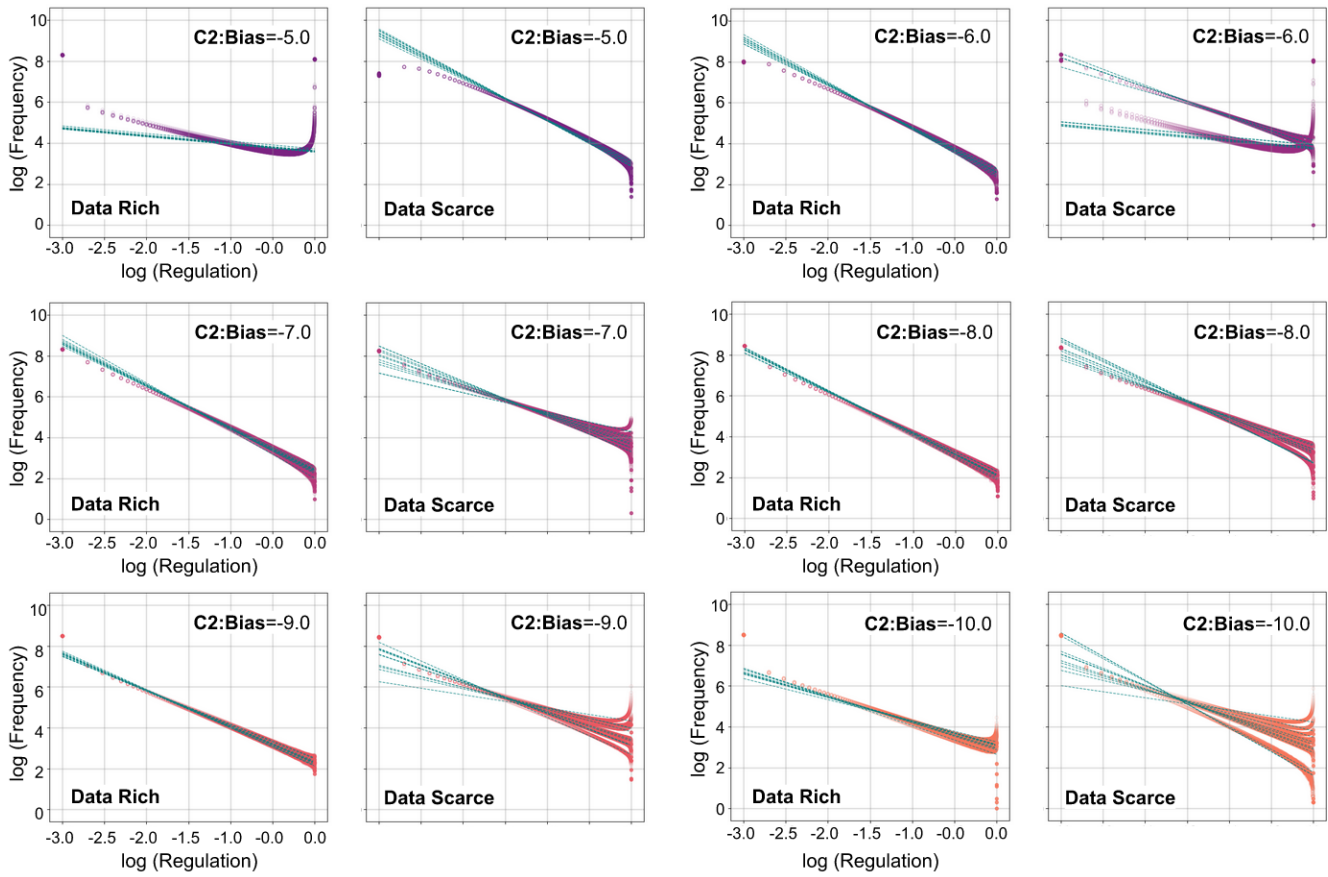


**Fig. 26.** We present individual log-log plots for regulation under domain transfer to ImageNet for each set of 10 runs per initial meta-learning bias setting for both data rich and data scarce meta-learning. These results continue in Fig.27. Qualitatively identical results for domain transfer to CIFAR-100 will be made available for download. But see Fig.29.



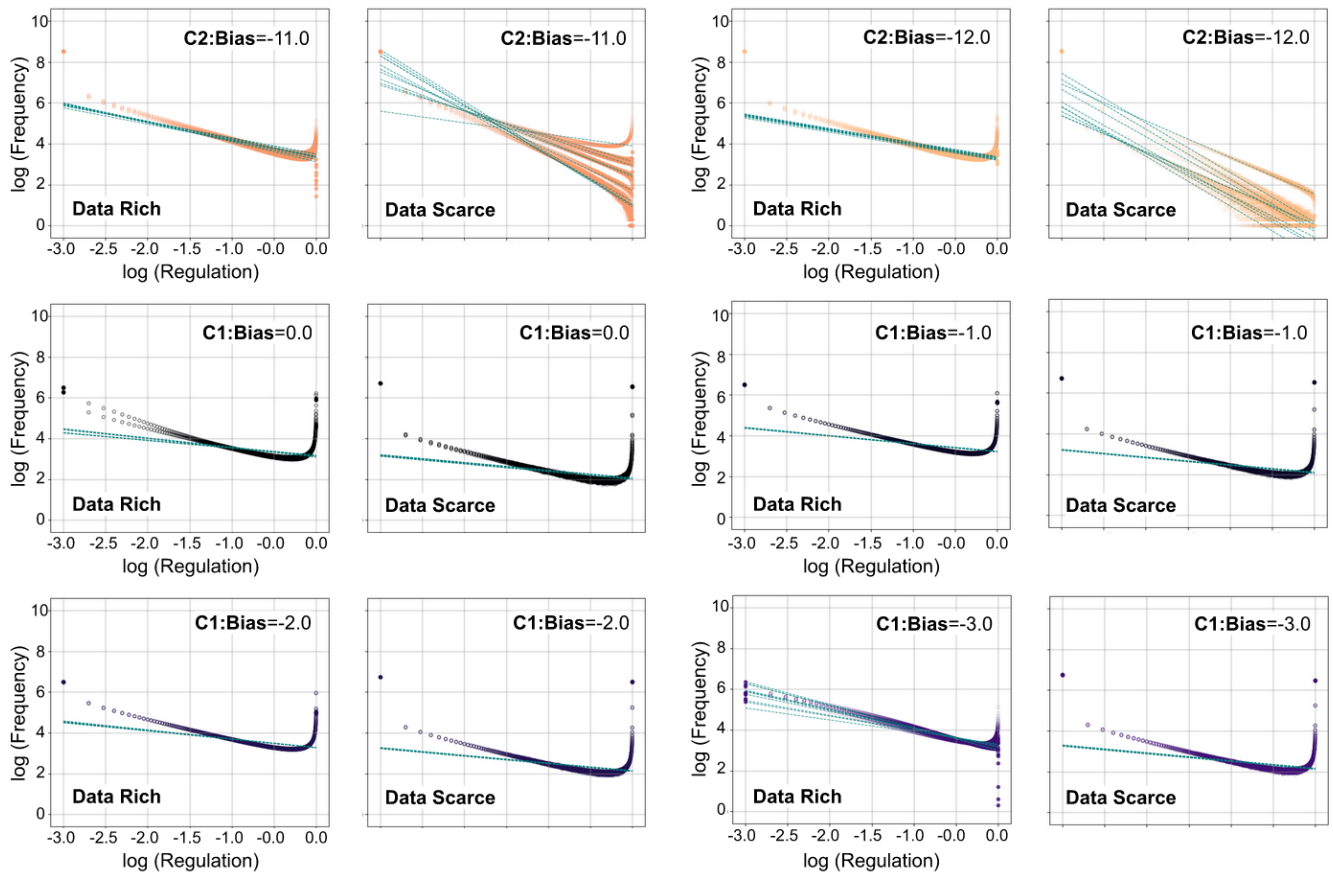


**Fig. 27.** We present individual log-log plots for regulation under domain transfer to ImageNet for each set of 10 runs per initial meta-learning bias setting for both data rich and data scarce meta-learning. These results continue in Fig.28. Qualitatively identical results for domain transfer to CIFAR-100 will be made available for download. But see Fig.29.

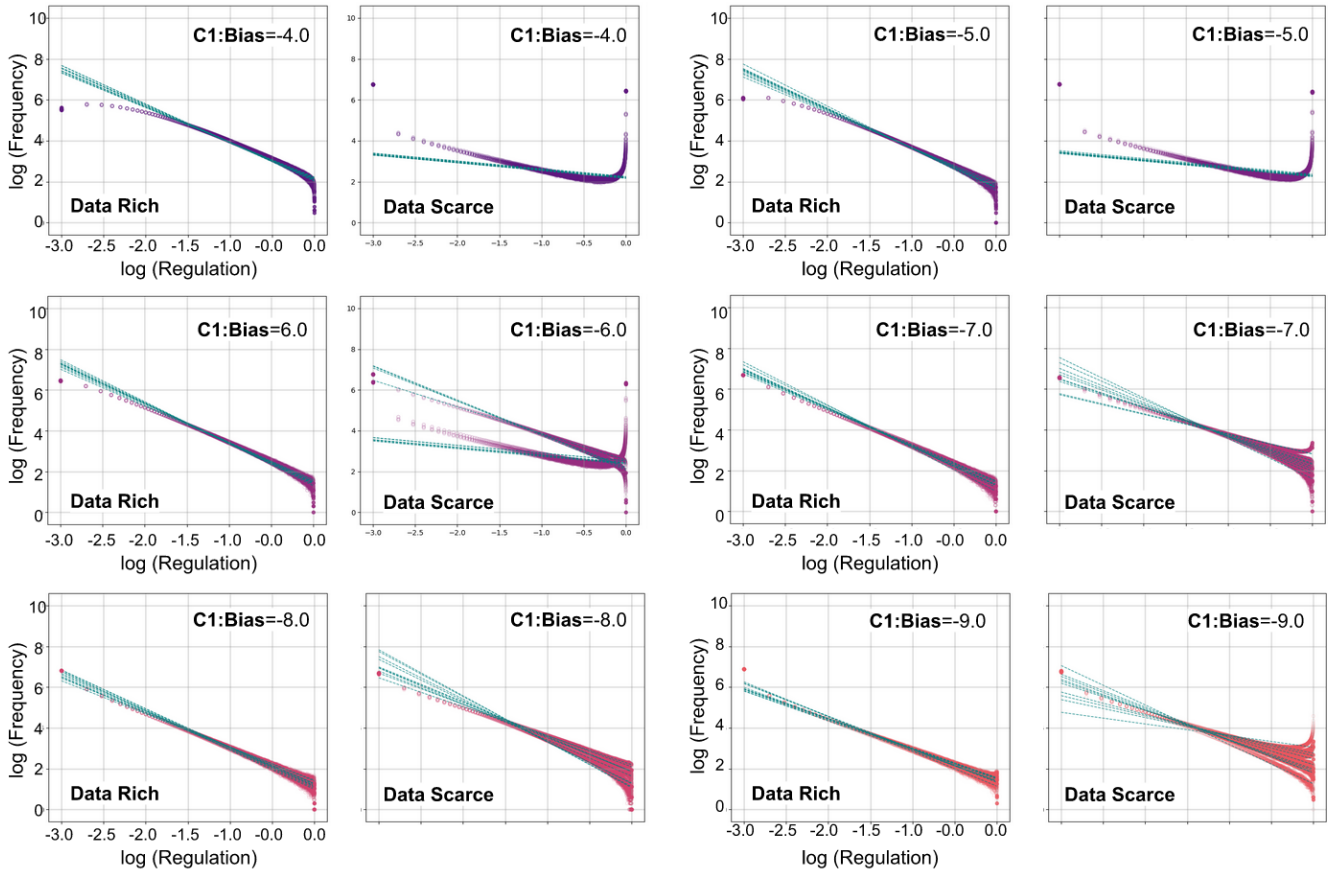


**Fig. 28.** We present individual log-log plots for regulation under domain transfer to ImageNet for each set of 10 runs per initial meta-learning bias setting for both data rich and data scarce meta-learning. These results continue in Fig.29. Qualitatively identical results for domain transfer to CIFAR-100 will be made available for download. But see Fig.29.

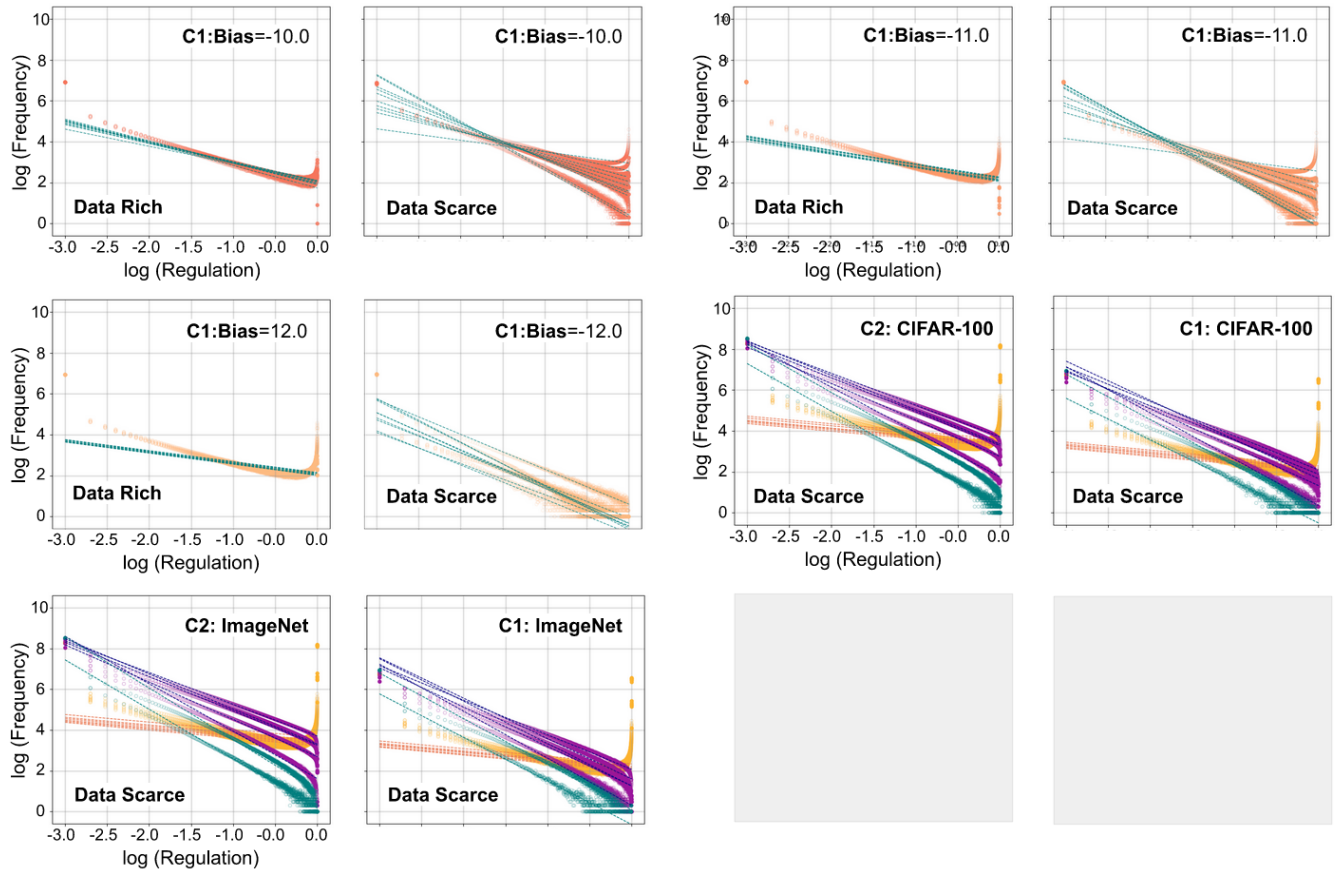


**Fig. 29.** We present individual log-log plots for regulation under domain transfer to ImageNet for each set of 10 runs per initial meta-learning bias setting for both data rich and data scarce meta-learning. Qualitatively identical results for domain transfer to CIFAR-100 will be made available for download. In the final four subplots, we show results for the stated layer and dataset for the best performing model in each setting of the initial meta-learning bias on regulation.